Journal of Medicinal Chemistry

pubs.acs.org/jmc

Article

Discovery of the Potent, Selective, Orally Available CXCR7 Antagonist ACT-1004-1239

Sylvia Richard-Bildstein,* Hamed Aissaoui, Julien Pothier, Gabriel Schäfer, Carmela Gnerre, Eleanor Lindenberg, François Lehembre, Laetitia Pouzol, and Philippe Guerry*

Cite This: https://dx.doi.org/10.1021/acs.jmedchem.0c01588

Read Online

ACCESS | Metrics & More | Article Recommendations | Supporting Information

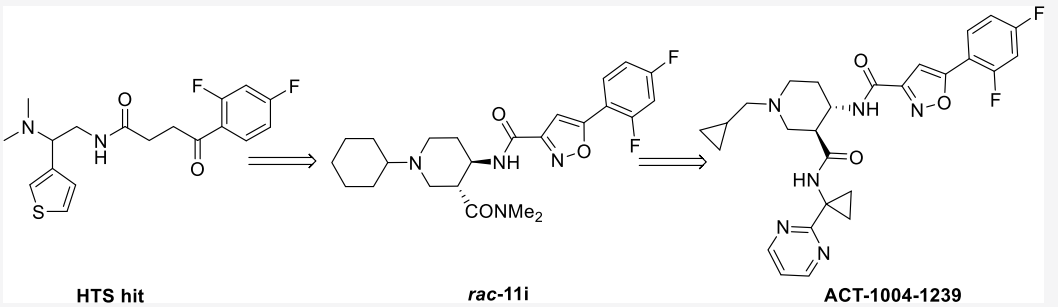

ABSTRACT: The chemokine receptor CXCR7, also known as ACKR3, is a seven-transmembrane G-protein-coupled receptor (GPCR) involved in various pathologies such as neurological diseases, autoimmune diseases, and cancers. By binding and scavenging the chemokines CXCL11 and CXCL12, CXCR7 regulates their extracellular levels. From an original high-throughput screening campaign emerged hit **3** among others. The hit-to-lead optimization led to the discovery of a novel chemotype series exemplified by the trans racemic compound **11i**. This series provided CXCR7 antagonists that block CXCL11- and CXCL12-induced ß-arrestin recruitment. Further structural modifications on the trisubstituted piperidine scaffold of **11i** yielded compounds with high CXCR7 antagonistic activities and balanced ADMET properties. The effort described herein culminated in the discovery of ACT-1004-1239 (**28f**). Biological characterization of ACT-1004-1239 demonstrated that it is a potent, insurmountable antagonist. Oral administration of ACT-1004-1239 in mice up to 100 mg/kg led to a dose-dependent increase of plasma CXCL12 concentration.

Downloaded via AUCKLAND UNIV OF TECHNOLOGY on December 14, 2020 at 17:46:19 (UTC).
See https://pubs.acs.org/sharingguidelines for options on how to legitimately share published articles.

INTRODUCTION

C-X-C chemokine receptor type 7 (CXCR7) is a seven-transmembrane G-protein-coupled receptor (GPCR), also known as ACKR3 (atypical chemokine receptor 3), expressed mainly by endothelial cells and other nonlymphoid cells, including mesenchymal cells, cardiomyocytes, neurons, astrocytes, and oligodendrocyte precursor cells (OPCs).[1,2] CXCR7 binds, internalizes, and degrades the chemokines CXCL11 (C-X-C chemokine ligand 11) and CXCL12 (C-X-C chemokine ligand 12). Importantly, CXCL11 and CXCL12 also bind to the chemokine receptors CXCR3 and CXCR4, respectively. Unlike classical GPCRs, CXCR7 does not couple with G proteins and consequently does not mediate signaling cascades but rather functions primarily as a scavenger receptor. Binding of its ligands leads to the recruitment of β-arrestin, internalization of the CXCR7-ligand complex,[1,3] and degradation of the ligand in lysosomes.[4] Through its scavenging function, CXCR7 regulates the extracellular levels of CXCL11 and CXCL12 and, therefore, modulates CXCR3 and CXCR4 activities.[5] CXCL11-CXCR3 signaling regulates migration, differentiation, and activation of immune cells including T helper type 1 cells and macrophages.[6−8] Activation of CXCR4 by CXCL12 mediates a wealth of cellular functions such as migration, adhesion, proliferation, differentiation, and cell survival.[9] Dysregulation of the CXCR7 axis has been associated with various disease states such as, neurological disorders,[10−13] autoimmune diseases,[14−17] inflammation,[18−20] cancers,[21−26] and cardiac disorders.[21,27,28]

Antibodies and/or small interfering RNA (siRNA) have demonstrated the utility of targeting CXCR7 in some of these diseases.[29−33] Although a number of small molecules were reported as CXCR7 antagonists,[17−19] they were later on described as bona fide agonists, recruiting β-arrestin to CXCR7 upon binding to the receptor ("functional antagonists").[34−36] Very recently, a moderately potent CXCR7 antagonist inhibiting the recruitment of ß-arrestin to CXCR7 following CXCL12 stimulation was reported ("true antagonist").[37] We describe here the hit-to-lead process followed by the lead

Received: September 10, 2020

ACS Publications

© XXXX The Authors. Published by American Chemical Society

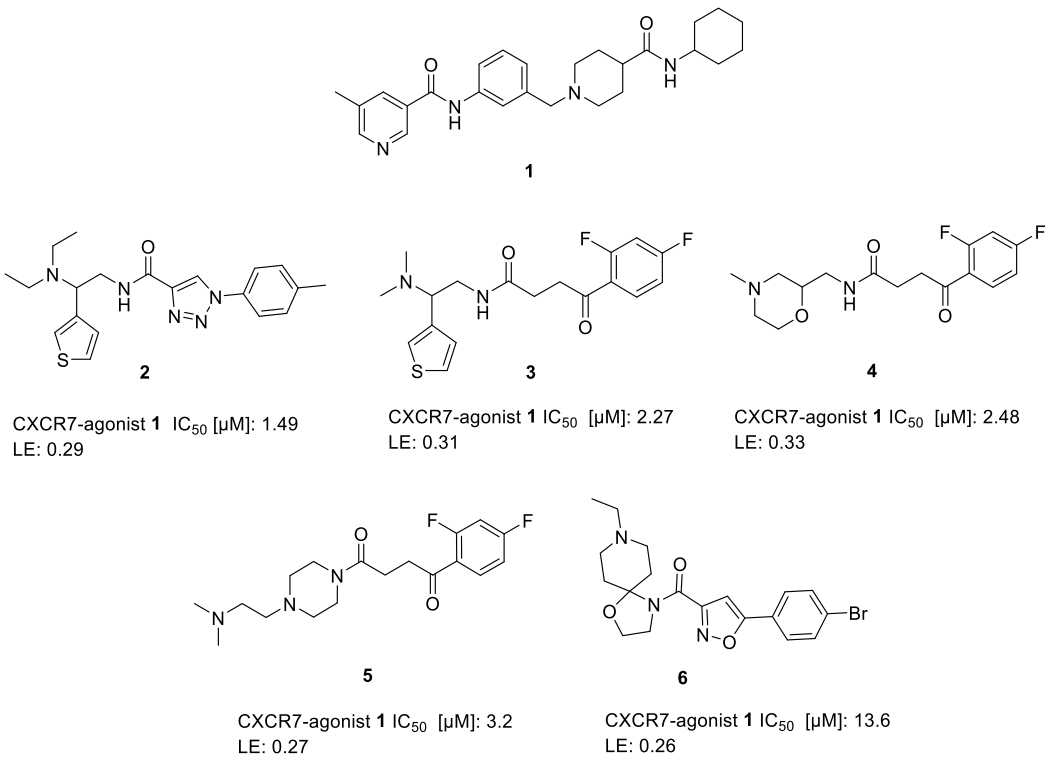

Figure 1. Structures of the CXCR7 agonist **1** and primary screening hits **2**–**6**.

optimization of a novel chemotype series providing potent, selective, insurmountable, and orally available "true" CXCR7 antagonists.

RESULTS AND DISCUSSION

Biological Assays. Binding of agonists to CXCR7 has been reported to mediate β-arrestin recruitment to the receptor. This recruitment can be monitored using the PathHunter CHO-K1 CXCR7 β-arrestin assay from DiscoverX ("CXCR7-agonist **1** assay" thereafter). The system is based on the enzyme fragment complementation technology. Two complementing fragments of the β-galactosidase (β-gal) enzyme are expressed within stably transfected cells. The larger portion of β-gal, termed EA for enzyme acceptor, is fused to the C-terminus of β-arrestin 2. The smaller fragment, termed ProLink tag, is fused to CXCR7 at the C-terminus. Upon activation, β-arrestin 2 is recruited to CXCR7, which forces the interaction of ProLink and EA, allowing complementation of the two fragments of β-gal, and the formation of a functional enzyme, which is able to hydrolyze the substrate and generating a chemiluminescent signal.

This assay was used to screen the Idorsia, formerly Actelion, screening compound collection. For practical and cost reasons, we decided to screen our library against the low-molecular-weight agonist **1**[38] (Figure 1) instead of the natural ligands CXCL11 and CXCL12. It was also postulated that this innovative approach could lead to the identification of weak antagonists that we might not have identified by screening against the natural ligands. The CHO-K1 CXCR7 β-arrestin cell line was preincubated with the compounds to be screened for 15 min before the addition of 5 nM of the small molecule agonist **1**. Compounds from our screening compound collection were screened at 10 μM. Compounds displaying more than 30% effect (inhibition) in the primary screen were selected, and their IC_{50} values were determined.

Following our screening cascade, another β-arrestin recruitment assay (CXCR7 Tango assay from Invitrogen, "CXCR7-CXCL12 assay" thereafter) was selected to further profile the active compounds using CXCL12 as a ligand. This assay was used as a biological *in vitro* assay to establish the SAR of the compounds identified in the primary screen. The CXCR7-β-lactamase U2OS cell line contains human CXCR7 fused at its intracellular C-terminus to the Gal4-VP16 transcription factor (CXCR7-Gal4-VP16). Interposed between CXCR7 and Gal4-VP16 is the tobacco etch virus (TEV) protease site that can be recognized and cleaved by the TEV protease. The parental cell line stably expresses a β-arrestin/TEV protease fusion protein and the β-lactamase reporter gene under the control of a UAS response element. Upon ligand binding and receptor activation, the protease-tagged β-arrestin molecule is recruited to CXCR7-Gal4-VP16. The protease cleaves the transcription factor Gal4-VP16 from CXCR7, which translocates to the nucleus and activates the expression of β-lactamase. A FRET-enabled substrate allows detecting β-lactamase activity. The results of this assay are reported as IC_{50} values.

Structure–Activity and Structure–Property Relationships. The 300,000 compounds of the HTS deck of Idorsia were composed of vendor screening compounds and proprietary compounds. The high-throughput screening of this compound collection against CXCR7 activated with the agonist **1**[38] (CXCR7-agonist **1** assay) identified a small cluster of five basic molecules **2**, **3**, **4**, **5**, and **6**, all of them devoid of antagonistic activity against the natural ligand in the CXCR7-CXCL12 assay. Herein, we describe the conversion of this unique cluster of antagonists active exclusively against the agonist **1** to potent CXCR7 antagonists active against the natural ligands CXCL11 and CXCL12.

https://dx.doi.org/10.1021/acs.jmedchem.0c01588
J. Med. Chem. XXXX, XXX, XXX–XXX

Table 1. First SAR Iteration on Amides A and B

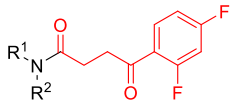

A

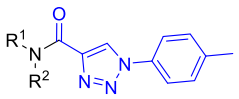

B

Compd	Amide	R^1R^2N-	CXCR7-agonist 1 IC_{50} [nM][a]	cLog $D_{7.4}$	LE
7a	A	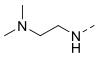	18600	0.47	0.32
7b	B	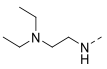	3100	-0.83	0.34
7c	A	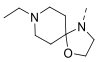	>10000	1.8	/
7d	B	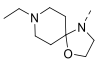	>10000	0.30	/
7e	B		3920	-0.16	0.32
7f	B	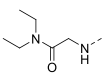	>10000	0.47	/
7g	B	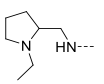	8280	0.11	0.30
7h	B	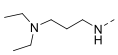	3050	-1.16	0.33
7i	A	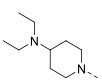	1670	0.76	0.32
7j	A	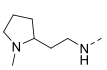	2720	0.91	0.33
7k	B	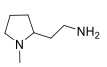	1280	-0.63	0.35
7l	A		3680	1.22	0.34
7m	A	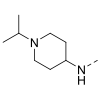	574	1.52	0.36
7n	B	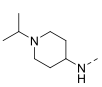	800	-0.01	0.35
7o	A	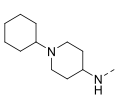	78	1.70	0.36
7p	B	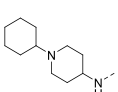	380	0.14	0.33

[a]The CHO-K1 CXCR7 β-arrestin cell line was preincubated with the compounds to be screened for 15 min before the addition of 5 nM of the small molecule agonist **1**, used as surrogate of endogenous CXCR7 ligands; data are the geometric mean (+/−2-fold) of at least three independent experiments. For synthesis and assay details, see the Supporting Information.

https://dx.doi.org/10.1021/acs.jmedchem.0c01588
J. Med. Chem. XXXX, XXX, XXX−XXX

Having no crystal structure of the target protein available to guide chemistry and in view of the structural features of the hits, a classical high-throughput chemistry approach was followed to explore the chemical space around these compounds using the CXCR7-agonist **1** assay. In the hit-to-lead phase of the project, several libraries were produced in an iterative manner starting mainly from commercially available building blocks. The five compounds depicted in Figure 1 shared some common features. To confirm the emerging SAR, two amide libraries have been prepared (Table 1). The truncation of the thiophene moiety in hits **2** and **3** (compounds **7a** and **7b**) led to similar or improved ligand efficiency (LE) showing that this moiety was not a key part of the pharmacophore. Combination of amine and carboxylic acid parts of the hits was either inactive (**7c**, **7d**) or equipotent (**7e**) to the original hits. As shown by the inactive compound **7f**, the basic amine seemed to be important for potency. Bridging of the tertiary amine to a pyrrolidine (**7g**) decreased the LE. The extension of the amide linker from two to three carbons led to similar (**7h**, **7j**) or improved LE (**7k**). Introduction of additional ring constraints in the linker was investigated. The 4-amino-piperidine cores of compounds **7i** and **7l** gave only a moderate LE, but the substitution of the piperidine N-atom with larger alkyl groups as analogs of **7l** provided a significant increase in potency with improved or at least similar LE as shown by compounds **7m** to **7p**, **7o** exhibiting an IC_{50} value of 78 nM. Considering the chemical structure of the compounds, a cardiac potassium channel hERG liability was anticipated and confirmed by the activity of **7o** in the hKV11.1 assay (IC_{50} = 4.7 μM). To minimize the risk of inhibition of this ion channel, the compounds were designed by ideally keeping the cLog $D_{7.4}$ in the range of 0.5−1.5.[39]

For the second synthetic iteration, 1-cyclohexylpiperidin-4-amine was kept constant and coupled with a series of carboxylic acids to map the right-hand side amide part (Table 2). An unsubstituted phenyl triazole **8a** and unsubstituted phenyl-4-oxobutanamide **8c** surprisingly led to a complete loss in activity, highlighting the importance of the substituents of the phenyl ring. It appeared that fluorine atoms had a synergistic effect and important role for reaching low nanomolar potency as shown by the *p*-fluorophenyl compound **8d** (IC_{50} = 374 nM, 5-fold less potent than **7o**). A *p*-bromo halogen atom was substantially less active (**8b**) and compound **8f** bearing a *p*-chloro substituent led to a 4-fold reduction in potency. A pyridine moiety as a bioisostere[40] of the 2,4-difluorophenyl group led to the inactive compound **8j**. The combination of an isoxazole and the key fluorine substituents as illustrated by compounds **8g**, **8h**, and **8i** gave an activity cliff to IC_{50} = 5 nM for **8g** and confirmed the important role of the two fluorine atoms. Based on the low nanomolar potency reached, compound **8g** was further characterized. Tested in the CXCR7-CXCL12 assay with CXCL12 as a ligand, **8g** showed an IC_{50} of 463 nM (Table 3). Despite an acceptable measured log $D_{7.4}$ of 2.8, **8g** showed an hERG inhibition of 1.5 μM in the hKV11.1 assay. But the compound exhibited encouraging solubilities in fasted (FaSSIF) and fed state simulated intestinal fluid (FeSSIF) with 144 and 196 mg/L, respectively, and an aqueous solubility of 15 mg/mL at pH 7.

For the next generation of compounds, the most potent ones were screened in the CXCR7-CXCL12 assay in addition to the CXCR7-agonist **1** assay. The left-hand part N-R^1 amine substituent was modified with the double aim of further improving the activity and tackling the identified hERG channel liability (Table 3). Diverse alkyl chains were tolerated and led to nanomolar activities in the CXCR7-agonist **1** assay. Unfortunately, the shift in IC_{50} between the CXCR7-agonist **1** assay and CXCR7-CXCL12 assay was still significant and the potency slightly decreased when the ring size was reduced (**9c** and **9d**). The amide analog **9a** confirmed that an amine group was mandatory for potency. In addition, attempts to reduce the basicity of the tertiary amine led also to a decrease in activity as depicted by the fluorinated example **9e** and ether analogue **9f**. A benzyl substituent **9g** led to the low IC_{50} shift of 12 between the assays but with the price of an increased lipophilicity and potentially an added metabolic hotspot. The shift observed with the secondary amine **9b** was the lowest (5.8), but the potency was too low for further investigation.

The replacement of the isoxazole ring with other 5-membered or 6-membered heterocycles was then explored. The modification had a marked impact on the lipophilicity of the compounds as shown by the clog $D_{7.4}$ values. Table 4

Table 2. Modulation of the Carboxamide Part

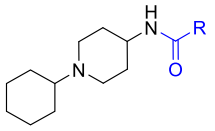

Compd	RCO-	CXCR7-agonist 1 IC_{50} [nM][a]	cLog D $_{7.4}$	LE
8a	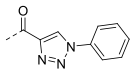	>10000	-0.2	/
8b	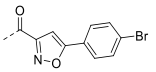	2010	1.9	0.29
8c	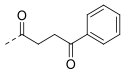	>25000	1.5	/
8d	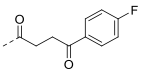	374	1.6	0.34
8e	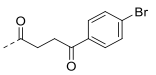	>25000	2.2	/
8f	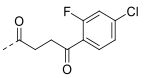	331	2.2	0.33
8g	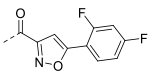	5	1.3	0.40
8h	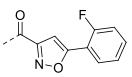	121	1.2	0.35
8i	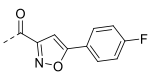	53	1.2	0.37
8j	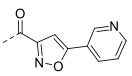	>10000	0.15	/

[a]The CHO-K1 CXCR7 β-arrestin cell line was preincubated with the compounds to be screened for 15 min before the addition of 5 nM of the small molecule agonist **1**, used as surrogate of endogenous CXCR7 ligands; data are the geometric mean (+/−2-fold) of at least three independent experiments. For synthesis and assay details, see the Supporting Information.

https://dx.doi.org/10.1021/acs.jmedchem.0c01588
J. Med. Chem. XXXX, XXX, XXX−XXX

Table 3. Exploration of the Tertiary Amine Moiety

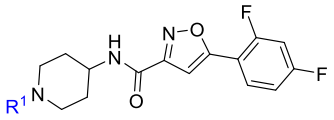

Compd	R1	CXCR7-agonist 1 IC_{50} [nM][a]	CXCR7-CXCL12 IC_{50} [nM][b,c]	IC_{50} shift	cLog D $_{7.4}$
8g		5	463	93	1.4
9a		>25000	nd	/	2.1
9b		548	3180	5.8	-0.9
9c		9	993	110	1.2
9d		9	1060	118	1.3
9e		5490	nd	/	2.2
9f	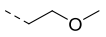	157	9480	60	1.0
9g	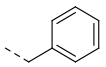	21	239	12	2.3

[a]The CHO-K1 CXCR7 β-arrestin cell line was preincubated with the compounds to be screened for 15 min before the addition of 5 nM of the small molecule agonist **1**, used as surrogate of endogenous CXCR7 ligands. [b]CXCR7-CXCL12 assay using CXCL12 as a ligand. [c]nd: not determined. Data are the geometric mean (+/−2-fold) of at least three independent experiments. For synthesis and assay details, see the Supporting Information.

depicts a selection of active molecules prepared. A decrease in affinity was observed for the pyrazole and triazole derivatives (**10a**, **10b**) in the CXCR7-agonist **1** assay. The inverted 3-(2,4-difluorophenyl)isoxazole analogue **10c** of **8g** was 5 times less potent in the CXCR7-agonist **1** assay but only 2 times less potent in the CXCR7-CXCL12 assay. Six-membered rings as exemplified by the pyrimidine **10f** led to a decrease in potency. Interestingly, the IC_{50} shift between the assays was in the same range for all these analogues and lower than observed previously. The oxadiazoles **10d** and **10e** showed potencies in the same range than **8g**, with IC_{50} values of 554 and 203 nM in the CXCR7-CXCL12 assay, respectively. Despite a measured log $D_{7.4}$ of 1.6, the latest compound did not exhibit an improvement on the hERG inhibitory activity with an IC_{50} of 2.7 μM.

As the SAR observed so far remained steep in the CXCR7-CXCL12 assay, it was decided to investigate the potential of a new exit vector on the 4-amino-piperidine core with the aim of further increasing activity in this assay and improving the selectivity over the hERG channel. All the compounds described in Table 5 are racemates unless otherwise stated, and their synthesis is described in the Supporting Information part.

Alkylation of the secondary amide function was rapidly abandoned due to a dramatic decrease in potency of the examples produced. Among them, only the benzyl analogue **11a** is shown. The focus was then set on the introduction of substituents in position 3 of the piperidine core. The decrease of the basicity of the tertiary amine by the addition of two fluorine atoms (**11b**) led to an important decrease in potency as observed previously (compound **9e**). The introduction of a methoxy group provided a significant improvement in potency as shown by compound **11c** with IC_{50} values of 2 nM in the CXCR7-agonist **1** assay and 61 nM in the CXCR7-CXCL12 assay. Larger alkoxy groups like ethoxy (**11d**) caused a loss in potency by 2-fold in both assays. The same exercise with a hydroxy group (**11e**) gave potencies in a similar low nanomolar range in the CXCR7-agonist **1** assay but a 2-fold potency decrease in the CXCR7-CXCL12 assay as compared with the methoxy analogue. Extending the alcohol function by one carbon (**11f**) did not improve the potency in the CXCR7-CXCL12 assay. The introduction of a methyl ester in position 3 of the piperidine core (**11g**) delivered a very potent compound in the CXCR7-agonist **1** assay that unfortunately exhibited a 100-fold IC_{50} shift in the CXCR7-CXCL12 assay. Saponification of the ester to the acid **11h**, which could have helped to modulate the hERG liability, caused a loss in

https://dx.doi.org/10.1021/acs.jmedchem.0c01588
J. Med. Chem. XXXX, XXX, XXX−XXX

Table 4. Exploration of the Core Heteroaromatic Ring

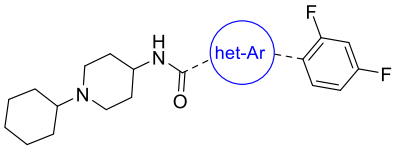

Compd	HetAr	CXCR7-agonist 1 IC_{50} [nM][a]	CXCR7-CXCL12 IC_{50} [nM][b,c]	IC_{50} shift	cLog D $_{7.4}$
10a	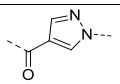	55	3160	57	0.2
10b	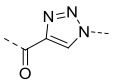	34	936	27	0.0
10c	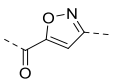	28	889	32	1.4
10d	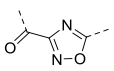	20	554	27	1.0
10e	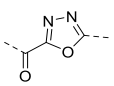	7	203	29	0.9
10f	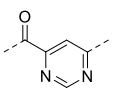	236	3060	13	1.3

[a]The CHO-K1 CXCR7 β-arrestin cell line was preincubated with the compounds to be screened for 15 min before the addition of 5 nM of the small molecule agonist **1**, used as surrogate of endogenous CXCR7 ligands. [b]CXCR7-CXCL12 assay using CXCL12 as a ligand. Data are the geometric mean (+/−2-fold) of at least three independent experiments. For synthesis and assay details, see the Supporting Information.

Table 5. Exploration of Exit Vectors and Substituents on the 4-Amino-piperidine Core

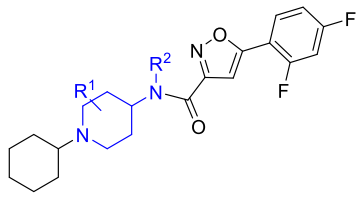

Compd	R^1 R^2	CXCR7-agonist 1 IC_{50} [nM][a]	CXCR7-CXCL12 IC_{50} [nM][b,c]	IC_{50} shift	cLog D $_{7.4}$
11a	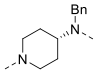	213	nd	/	3.1
11b	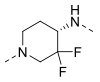	611	nd	/	3.7
11c	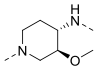	2	61	30	1.3
11d	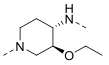	5	122	24	1.7
11e	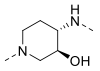	2	123	61	0.93
11f	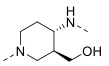	5	324	65	0.81
11g	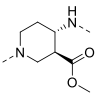	2	206	103	1.2
11h	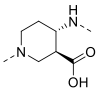	138	1620	12	-2.1
11i	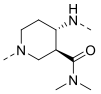	1.5	66	23	0.5
(*R*,*R*)-11i	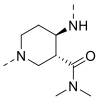	1.5	37.6	25	0.5
(*S*,*S*)-11i	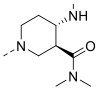	7.4	388	52	0.5
11j	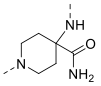	>25000	nd	/	0.22

[a]The CHO-K1 CXCR7 β-arrestin cell line was preincubated with the compounds to be screened for 15 min before the addition of 5 nM of the small molecule agonist **1**, used as surrogate of endogenous CXCR7 ligands. [b]CXCR7-CXCL12 assay using CXCL12 as a ligand. [c]nd: not determined. Data are the geometric mean (+/−2-fold) of at least three independent experiments. For synthesis and assay details, see the Supporting Information.

potency. Interestingly, by the introduction of a dimethyl amide, the potency was regained as shown by compound **11i** that exhibited an IC_{50} of 66 nM in the CXCR7-CXCL12 assay. The shift of the amide group to position 4 of the piperidine core exemplified by the achiral compound **11j** led to a complete loss in activity.

Compound **11i** was selected for further characterization. Aqueous solubility (192 mg/L at pH 7) and solubilities in FaSSIF and FeSSIF (569 and 652 mg/L) were improved compared to **8g**. Some ADMET parameters were promising, especially with an intrinsic clearance of 13 μL/min/mg protein in human microsomes and 274 μL/min/mg protein in rat microsomes. Finally, compound **11i** demonstrated moderate inhibitory potency (IC_{50} = 5.5 μM) in the hKV11.1 assay. Separation of the racemate **11i** by chiral prep. HPLC delivered both enantiomers (*R*,*R*)-**11i** and (*S*,*S*)-**11i**, which, respectively, display IC_{50} CXCR7-agonist **1** assay/IC_{50} CXCR7-CXCL12 assay of 1.5 nM/37.6 nM and 7.4 nM/388 nM. A 5-fold shift in the CXCR7-agonist **1** assay and a 10-fold shift in the CXCR7-CXCL12 assay were observed between both enantiomers, highlighting that the influence of the absolute stereochemistry had to be assessed. The absolute stereochemistry of enantiomers (*R*,*R*)-**11i** and (*S*,*S*)-**11i** was confirmed by an enantioselective synthesis described in the chemistry part.

https://dx.doi.org/10.1021/acs.jmedchem.0c01588
J. Med. Chem. XXXX, XXX, XXX−XXX

Table 6. SAR of 3-Carboxamide Moiety of the *trans* Racemic Series

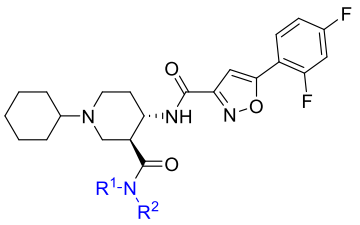

Compd	-NR^{1}R^2	CXCR7-CXCL12 IC$_{50}$ [nM][a]	cLog D$_{7.4}$
20a		156	-0.06
20b		82	0.27
20c		118	1.0
20d		201	1.0
20e		764	1.4
20f	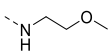	282	0.47
20g	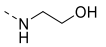	429	-0.18
20h	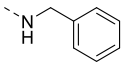	36	1.7
20i	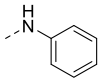	968	2.1
20j	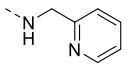	51	0.85
20k	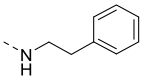	2.7	2.2
20l	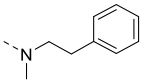	10	2.4
20m	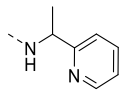	6.7	1.2
20n[b]	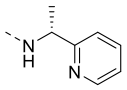	353	1.2
20o[c]	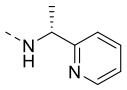	3.2	1.2
20p[b]	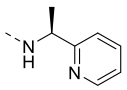	410	1.2
20q[c]	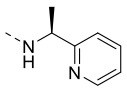	981	1.2

[a]CXCR7-CXCL12 assay using CXCL12 as a ligand. [b]Separated (3*R*,4*R*) enantiomer. [c]Separated (3*S*,4*S*) enantiomer. Data are the geometric mean (+/−2-fold) of at least three independent experiments.

To ensure a sustainable antagonistic effect, the ideal compound should be insurmountable, meaning that its potency should be constant even in the presence of potentially increasing concentrations of the natural ligands. A selection of compounds was tested in an insurmountability assay (Supporting Information). Whereas compounds **11c** and **11e** were found surmountable, the (*R*,*R*)-enantiomer of the dimethyl analog **11i** was the first compound showing insurmountability. This exciting finding encouraged us to investigate further this exit vector and to produce large amide libraries from the racemic *trans* carboxylic acid intermediate **11h**. Some of the most interesting analogs are shown in Table 6.

The coupling with diverse small alkyl amines (**20a**−**20d**) gave compounds with potencies in a similar range than the dimethylamide **11i** in the CXCR7-CXCL12 assay. The introduction of cyclic secondary amines led to a 3- and 10-fold decrease in potency for the azetidine (**20d**) and the pyrrolidine (**20e**), respectively. More hydrophilic groups did not improve potency as shown by compounds **20f** and **20g**. Interestingly, the coupling with amines bearing an aromatic group gave a significant increase in potency as depicted by the benzylamide **20h** with an IC$_{50}$ of 36 nM and the pyridin-2-yl-methanamide **20j** with an IC$_{50}$ of 51 nM. The phenylamide **20i** was less potent. A further surprising breakthrough was achieved with the phenethyl amides **20k** and **20l** with low nanomolar potencies for the first time of IC$_{50}$ = 10 nM and IC$_{50}$ = 2 nM, respectively. Another major improvement was realized when the pyridin-2-yl-methanamide **20j** was shielded with a methyl group at the benzylic position. Indeed, compound **20m**, a mixture of four *trans*-diastereomers showed a 10-fold increase in potency with an IC$_{50}$ of 6.7 nM.

Having established the absolute stereochemistry of (3*S*,4*S*)-**11i** and (3*R*,4*R*)-**11i**, the same exercise was repeated with both enantiomeric (*R*)-1-pyridinyl-2-yl-ethylamine and (*S*)-1-pyridinyl-2-yl-ethylamine that were coupled with both enan-

https://dx.doi.org/10.1021/acs.jmedchem.0c01588
J. Med. Chem. XXXX, XXX, XXX−XXX

Table 7. Structural Modification and Properties: 3-Carboxamide Moiety

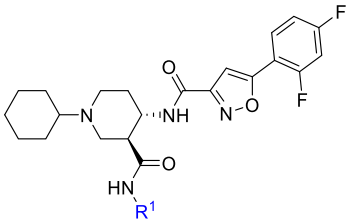

Compd	R^1	CXCR7-CXCL12 IC_{50} [nM][a]	Log $D_{7.4}$	HLM Cl_{int}[μL/min/mg]	hPPB [%]	hERG IC_{50}
20o	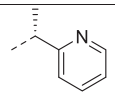	3.2	3.9	100	93.1	3.4
21a	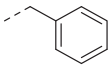	49	>4.1	67	nd[b]	>10
21b	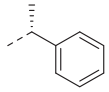	5.5	>4.1	149	98.4	>10
21c	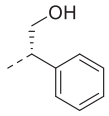	43.1	4.0	76	nd	7.2
21d	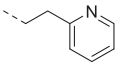	8.7	3.6	134	92.8	0.96
21e	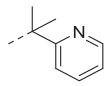	0.37	3.8	78	92.9	1.5
21f	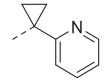	4.2	> 3.8	47	93.0	>10
21g	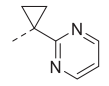	0.75	2.9	22	84.1	2.6

[a]CXCR7-CXCL12 assay using CXCL12 as a ligand. [b]nd: not determined. Data are the geometric mean (+/−2-fold) of at least three independent experiments.

tiomers (*S,S*)-**19** and (*R,R*)-**19** intermediates to deliver the four possible *trans*-enantiomers. The diastereomer **20o** was the most potent antagonist of this series, followed by **20n**, then **20p**, and finally **20q**. Compound **20o** was selected for further characterization. Its aqueous solubility was low (4 mg/L at pH 7), whereas solubility values in FaSSIF and FeSSIF were 38 and > 910 mg/L, respectively. Several ADMET parameters were not yet optimal, especially CL_{int} in HLM (100 μL/min/mg) and in RLM (823 μL/min/mg). On the other hand, compound **20o** still demonstrated inhibitory potency (IC_{50} = 3.4 μM) in the hERG assay. **20o** was also found insurmountable. Stereochemistry of the central scaffold appeared to play an important role in combination with the substitution on the 3-carboxamide, a large amide group being more potent when combined with the (*S,S*) scaffold. On the other hand, a small dimethyl amide combined with the (*R,R*) scaffold was more potent than the corresponding (*S,S*) analogue as shown before (compound (*R,R*)-**11i**). As replacement of the dimethyl amide with other small amides did not improve the potency, the focus was to further improve potency and properties for oral administration by exploring (*S,S*)-3-carboxamides containing an aromatic or heteroaromatic ring.

The *in vitro* characteristics of this panel of 3-carboxamides are detailed in Table 7. The (*S,S*)-benzylic analogue **21a** displayed the same potency as the racemic **20h**. Methylation of the benzylic position improved the potency further but increased the lipophilicity, which translated in a decreased metabolic stability. Further structural modifications were attempted to reduce lipophilicity and thereby increase metabolic stability. Hydroxylation on the benzylic methyl group (**21c**) reduced the potency. Spacer extension was tolerated but **21d** was rather metabolically unstable. The dimethylated compound **21e** was very potent. The 1-(pyridin-2-yl)cyclopropyl amide **21f** was slightly less potent but not inhibiting the hERG channel up to 10 μM in comparison to many analogues of this series, and it exhibited a metabolic stability of 47 μL/min/mg. Finally, the 1-(pyrimidin-2-

https://dx.doi.org/10.1021/acs.jmedchem.0c01588
J. Med. Chem. XXXX, XXX, XXX−XXX

Table 8. Structural Modification and Properties: *N*-1-Piperidine Substituents

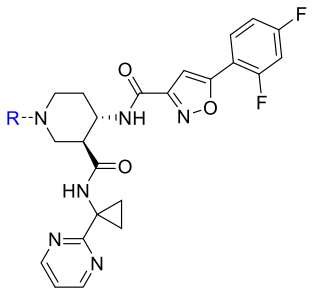

Compd	R	CXCR7-CXCL12 IC_{50} [nM][a]	Log $D_{7.4}$	pKa	HLM Cl_{int}[μL/min/mg]	hPPB [%]	hERG IC_{50}
27		169	0.6	8.1	22	nd[b]	>10
28a		111	1.7	7.3	18	nd	>10
28b		48	1.8	7.6	<10	75.4	>10
28c		18.4	2.5	7.6	14	77.9	4.4
28d		20.5	1.8	8.0	<10	73.1	>10
28e		554	2.4	6.1	21	nd	>10
28f		3.2	2.5	7.7	9.2	88.4	5.7
28g		25	2.9	7.4	17	82.9	>10
28h		0.6	3.1	7.7	50	91.5	1.4
28i		1.9	2.9	7.6	24	86.2	9.6
28j		2.7	3.1	7.5	148	95.7	11
28k		24	2.7	6.2	22	89.0	>10
28l		85	2.2	6.8	16	nd	>10
28m		975	2.9	5.2	nd	nd	>10
28n		49.2	1.9	6.7	21	nd	>10
28o		1120	1.6	<2	nd	nd	>10

[a]CXCR7-CXCL12 assay using CXCL12 as a ligand. [b]nd: not determined. Data are the geometric mean (+/−2-fold) of at least three independent experiments.

yl)cyclopropyl amide **21g** was a very potent antagonist, displaying a metabolic stability of 22 μL/min/mg but inhibiting hERG with an IC_{50} of 2.6 μM. Protein binding was measured in human plasma for the most promising antagonists and found to be in a range of 84.1−98.4%. This exploration of the amide substitution of the 3-carboxamide led to the identification of very potent antagonists, however with moderate Cl_{int} values in HLM and still showing hERG inhibitory activities.

Table 8 summarizes the impact of *N*-substitution on the potency, the Cl_{int} in HLM, the IC_{50} against the hERG channel, and on some additional physico-chemical properties. These modifications showed that the lipophilicity of substituents was an important feature for low nanomolar potency on the receptor, small substituents like H (**27**), Me (**28a**), or ethyl (**28b**) giving less potent compounds. On the other hand, larger substituents gave compounds that displayed higher Cl_{int} values in HLM and had a stronger affinity toward hERG. Basicity of

https://dx.doi.org/10.1021/acs.jmedchem.0c01588
J. Med. Chem. XXXX, XXX, XXX−XXX

Scheme 1. Preparation of (3*S*,4*S*)-1-Cyclohexyl-4-{[carboxyamino-3-carbonyl]-amino}-piperidine-3-carboxylic Acid-amide Derivatives (3*S*,4*S*)-11i[a]

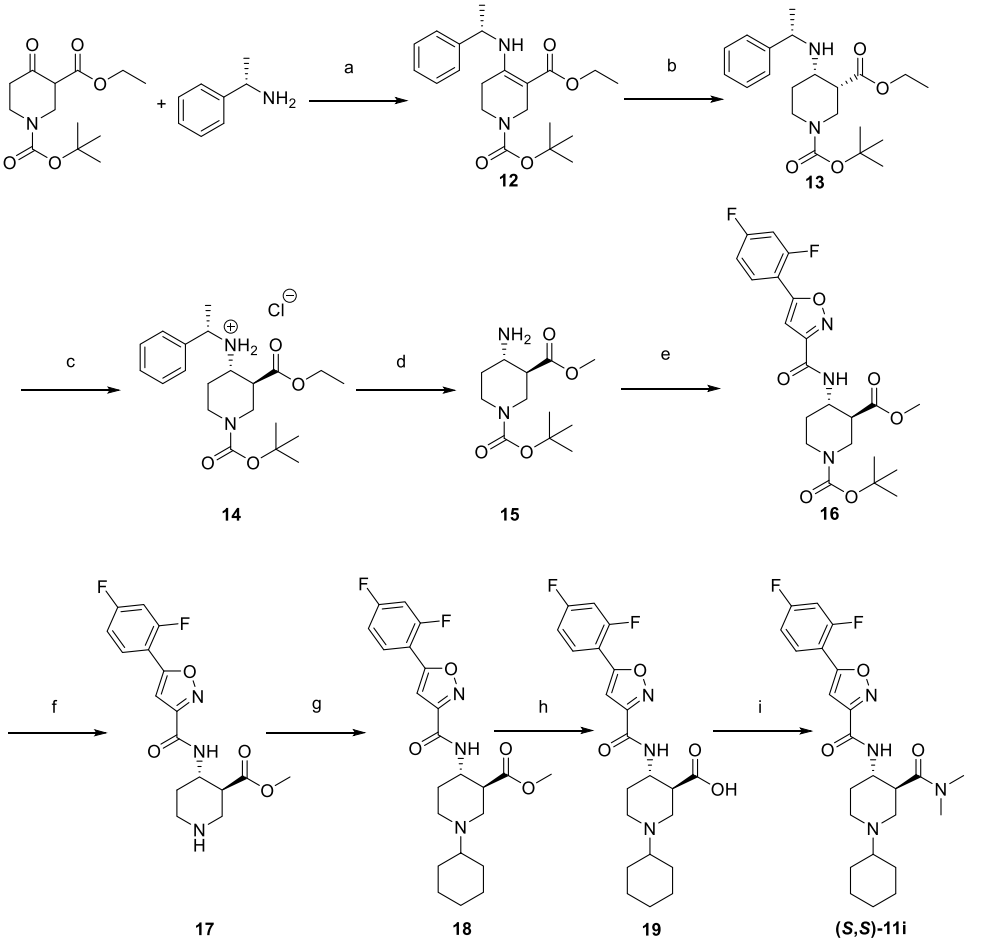

[a]Reagents and conditions: (a) *p*-toluensulfonic acid, toluene, reflux, 18 h, quantitative; (b) $NaBH_4$, isobutyric acid, toluene, 0 °C, 6 h; (c) NaOEt, EtOH, 50 °C, 18 h, then HCl diethylether/dioxane, 16%; (d) 10% Pd/C, HCO_2NH_4, MeOH, reflux, 2 h, 82%; (e) 5-(2,4-difluoro-phenyl)-isoxazole-3-carboxylic acid, HATU, DIPEA, DMF, rt., 18 h, 51%; (f) HCl 4 N in dioxane, DCM, rt., 30 min, 99%; (g) cyclohexanone, $NaBH(OAc)_3$, AcOH, DCM, rt., 24 h, 94%; (h) NaOH aq., THF, rt., 6 h, quantitative; and (i) dimethylamine, (40% in water), HATU, DIPEA, DMF, rt., 6 h, 36%.

the piperidine nitrogen was measured through the pK_a of the conjugated acid. The nitrogen needed to be basic enough for highly potent CXCR7 antagonism. The corresponding neutral *N*-acetamide **28o** was indeed only weakly active. Introduction of fluorine in compounds **28k**, **28l**, **28m**, or of a methoxy group as in derivative **28n** on the *N*-alkyl substituent did reduce the basicity and the hERG blockage but at the same time reduced the affinity to the receptor. Protein binding was measured in human plasma for the most promising antagonists and was in a range of 73.1−91.5%. Among all the compounds of Table 8, the *N*-cyclopropylmethyl compound **28f** displayed the most balanced profile.

The interesting profile of **28f** prompted us to confirm the influence of stereochemistry on the antagonist potency. The stereochemistry had a strong impact as the corresponding *trans*-(3*R*,4*R*)-enantiomer **29**, obtained by the same synthetic approach and is described in Scheme 2 but starting with the chiral auxiliary (*R*)-(+)-α-methylbenzylamine, was 150 time less potent with an IC_{50} of 490 nM. This stereochemical effect was even more pronounced in the case of the *cis* substitution as both *cis*-(3*R*,4*S*)-**30** and *cis*-(3*S*,4*R*)-**31** enantiomers were found to be rather weak antagonists with IC_{50} of 2250 nM and above 5500 nM, respectively. The *cis* enantiomers **30** and **31** were obtained from the same synthetic pathway and are described in Scheme 2, starting either from (*S*)-(−)-α-methylbenzylamine or (*R*)-(+)-α-methylbenzylamine, without conducting the equilibration step. The structural assignment based on the synthetic access,[41] in particular the absolute (3*S*,4*S*) stereochemistry, was confirmed by X-ray analysis of crystals of compound **28f** (Figure 2).

To summarize the important features *in vitro*, potent antagonists required some basic character on N-1 of the piperidine and sufficient lipophilicity to achieve a low nanomolar potency on the target receptor. Ideal basicity values were found to be close to pKa 7.4 to keep potency on the receptor and should not be higher than pKa 7.8 to avoid stronger hERG inhibition. Lipophilicity (log $D_{7.4}$) was kept below 2.7 for the same reasons. Despite the surprisingly narrow navigation space between these molecular properties, compound **28f**, named with the corporate code ACT-1004-1239, fitted most requirements and was therefore selected as the ideal candidate for *in vivo* evaluation. Compound **28f** is a weak base (pK_a = 7.7) and displays an aqueous solubility of 374 mg/L at pH 7, whereas solubility values in FaSSIF and FeSSIF

https://dx.doi.org/10.1021/acs.jmedchem.0c01588
J. Med. Chem. XXXX, XXX, XXX−XXX

Scheme 2. Preparation of 1-Substituted (3S,4S)-4-{[5-(2,4-Difluoro-phenyl)-isoxazole-3-carbonyl]-amino}-piperidine-3-carboxylic Acid (1-Pyrimidin-2-yl-cyclopropyl)-amide Derivatives[a]

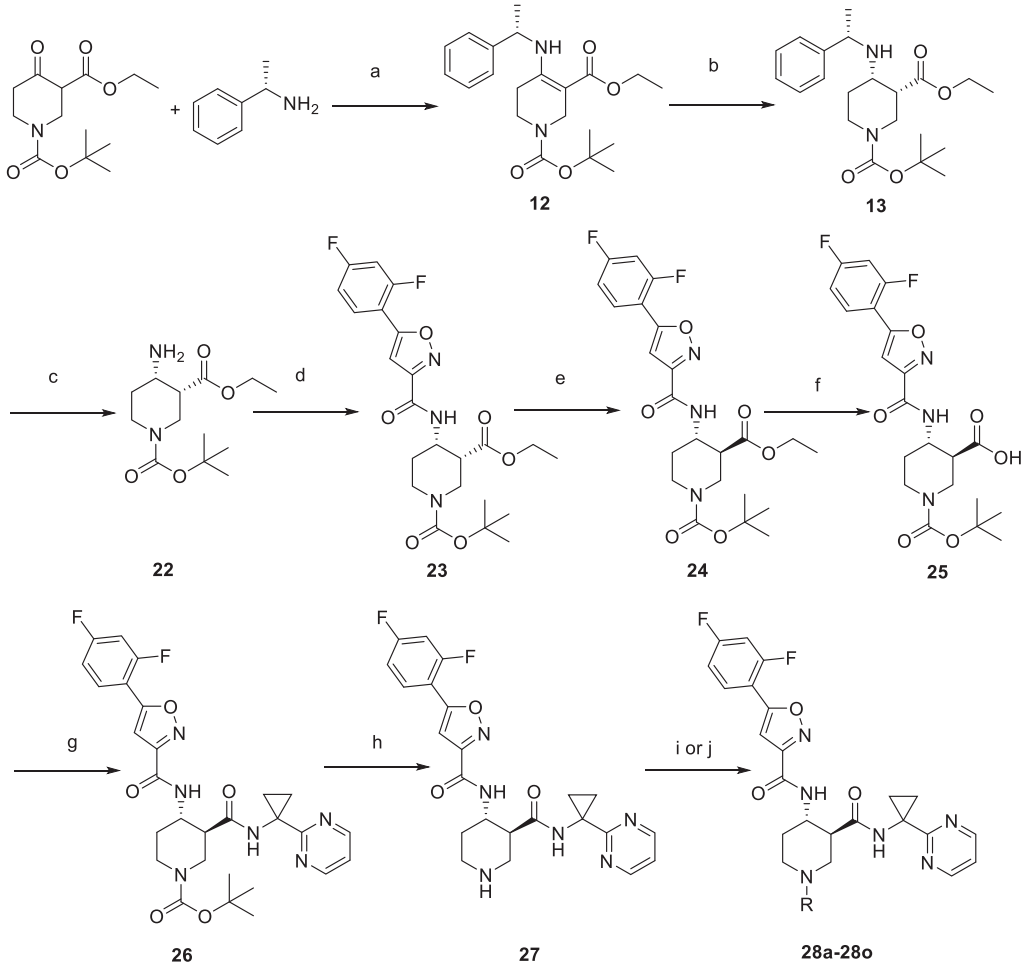

[a]Reagents and conditions: (a) *p*-toluensulfonic acid, toluene, reflux, 18 h, quantitative; (b) $NaBH_4$, trifluoracetic acid, THF, −18 °C, 1 h; (c) 20% $Pd(OH)_2/C$, H_2, MeOH, rt., 18 h, quantitative; (d) 5-(2,4-difluoro-phenyl)-isoxazole-3-carboxylic acid, T_3P, DCM, TEA, rt., 18 h, 79%; (e) NaOEt, EtOH, EtOAc, rt., 2 h, chiral chromatography, 63%; (f) NaOH 1 N aq., THF, rt., 8 h, HCl 2 N, rt., 30 min, 98%; (g) 1-pyrimidin-2-yl-cyclopropylamine, HATU, DIPEA, DMF, rt., 18 h, 87%; (h) 4 N HCl in 1,4-dioxane, MeOH, rt., 1 h, $NaHCO_3$ aq. DCM, 98%; (i) aldehyde or ketone, $NaBH(OAc)_3$, AcOH, DCM, rt., 24 h, 94%; and (j) alkyl bromide or iodide, base, acetone.

were 513 and > 880 mg/L. The capacity of **28f** to inhibit the cytochrome P450 2C9, 2D6, and 3A4 was assessed *in vitro* in HLM. All IC_{50} values were above 50 μM. ACT-1004-1239 was very potent on CXCR7 from other species and inactive on human CXCR4 (Table 9). ACT-1004-1239 was tested in a panel of 87 enzymatic and radioligand binding assays and was found to be selective for CXCR7 (data not shown).

Insurmountability Assessment and Binding Kinetic of ACT-1004-1239. We then wished to confirm that ACT-1004-1239 displayed insurmountable antagonism against both CXCR7 ligands, CXCL11 and CXCL12. Thus, the IC_{50} of ACT-1004-1239 was determined in the presence of increasing concentrations of CXCL11 or CXCL12 (up to 1 μM). As shown in Figure 3, the IC_{50} values of ACT-1004-1239 fell into a narrow range at different ligand concentrations. The data show that ACT-1004-1239 is a potent insurmountable CXCR7 antagonist against both CXCL11 and CXCL12.

To determine the association (K_{on}) and dissociation (K_{off}) rate constants of ACT-1004-1239, a HEK293 cell line expressing a SNAP-tag-fused hCXCR7 receptor was established for the binding assay. Cells stably expressing the SNAP-tag-hCXCR7 fusion protein were labelled with SNAP-Lumi4-Tb. A fluorescent derivative of CXCL12, hereafter named "red-CXCL12", was used. The dissociation constant (K_d) of red-CXCL12 was determined to be 1.33 nM at room temperature (data not shown). Competitive binding assays were carried out using ACT-1004-1239 as a competitor. As expected, Figure 4 shows a decrease of the HTRF signal upon the addition of increasing concentrations of ACT-1004-1239. In this experiment, ACT-1004-1239 had a K_i of 0.53 nM, a K_{off} of 0.06945 min^{-1}, and a K_{on} of 1.309 10^8 M^{-1} min^{-1} at room temperature.

The dissociation rate constant of ACT-1004-1239 (residence time, $t = 1/K_{off}$) was 14.4 min, and its half-life ($t_{1/2} = \ln 2/K_{off}$) was 9.98 min.

***In Vivo* Pharmacokinetic Studies.** Pharmacokinetic studies were performed in rat and dog after oral (10 and 1 mg/kg) and intravenous (1 mg/kg) dosing. The pharmacokinetic parameters of ACT-1004-1239 are described in Table 10, which also displays the plasma protein binding and intrinsic clearance in the liver microsomal preparation of each species. After intravenous dosing in the rat, ACT-1004-1239 displayed a systemic plasma clearance of 70 mL/min per kilogram. After

https://dx.doi.org/10.1021/acs.jmedchem.0c01588
J. Med. Chem. XXXX, XXX, XXX−XXX

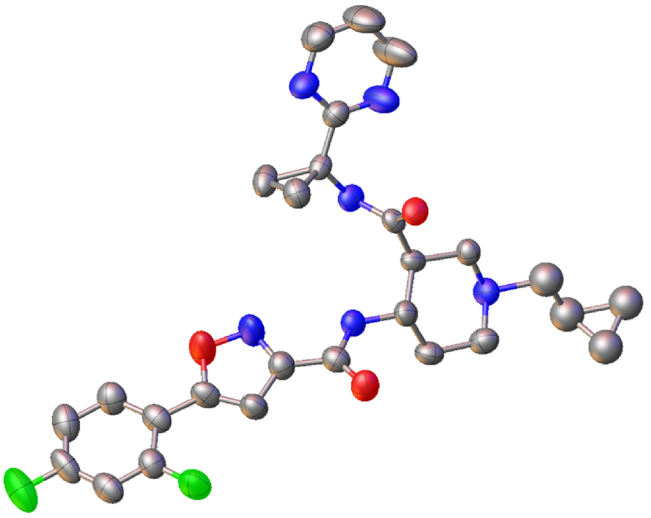

Figure 2. Molecular structure of compound **28f** as determined by X-ray structural analysis. Anisotropic thermal ellipsoids are drawn at a 50% probability level. The cyclopropyl rest was not refined anisotropically (due to a high disorder present, for details see the Experimental Section and Supporting Information). For clarity, the disordered part and all hydrogen atoms have been omitted. The solvate molecule present (MeOH) was squeezed using software tool Platon SQUEEZE.[44]

Table 9. *In Vitro* Pharmacology of ACT-1004-1239 (28f)[a]

human CXCR7[a] IC_{50} (nM)	3.2
dog CXCR7[b] IC_{50} (nM)	2.3
rat CXCR7[c] IC_{50} (nM)	3.1
mouse CXCR7[d] IC_{50} (nM)	2.3
guinea pig CXCR7[e] IC_{50} (nM)	0.6
macaque CXCR7[f] IC_{50} (nM)	1.5
human CXCR4[g] IC_{50} (nM)	>10000

[a]Note: [a]CXCR7-CXCL12 assay. [a−f]Assays performed with CXCL12 as a ligand. [b−f]Data are the average of at least five independent experiments and were determined using the DiscoverX assay. [g]Human CXCR4 FlipR assay. For assay details, see the Supporting Information.

correction for blood/plasma partitioning, blood clearance was approximatively 70% of the liver blood flow. Plasma and blood clearances in the dog were 2.8 and 3.8 mL/min per kilogram, the latter representing 9% of the liver blood flow. These data show that ACT-1004-1239 is a high-clearance drug in the rat and a low-clearance drug in the dog. Also, these *in vivo* clearance data are in line with the *in vitro* intrinsic clearance values determined in rat and dog liver microsomes, i.e., of 140 versus 5 μ/mL per milligram protein, respectively. The volume of distribution at the steady state (V_{ss}) in rat and dog was in excess of total body water with 3.6 and 1.6 L per kilogram, respectively. Oral absorption was rapid in the rat with peak plasma concentrations being reached within 0.5 h. In the dog, T_{max} was around 1.5 h. Bioavailability reached 35% in the rat and was 61% in the dog.

Evaluation of *in Vivo* Target Engagement. The potency and rodent pharmacokinetic properties of compound ACT-1004-1239 administrated orally were suitable for evaluating this compound *in vivo*. The effect of ACT-1004-1239 on plasma CXCL12 was evaluated in naive male DBA/1 mice at a range of 1−100 mg/kg. Single oral dosing resulted in a rapid, significant, dose-dependent increase in CXCL12 plasma

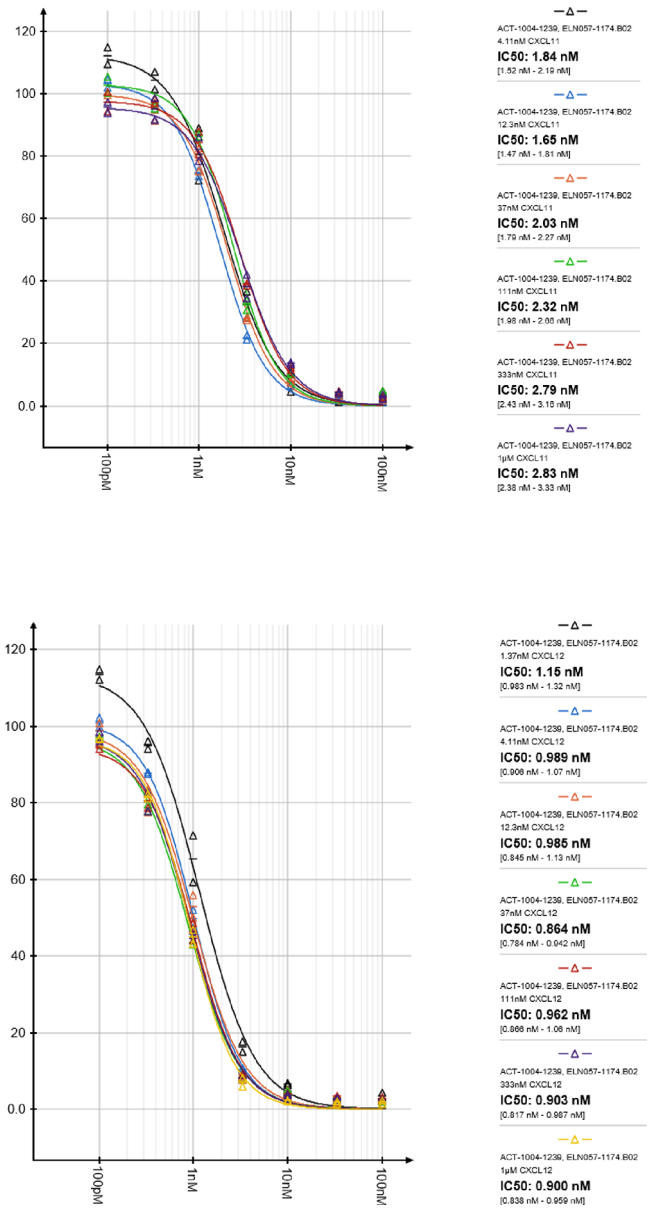

Figure 3. Determination of ACT-1004-1239 insurmountability against CXCL11 (upper panel) and CXCL12 (lower panel) in the CXCR7-agonist **1** assay.

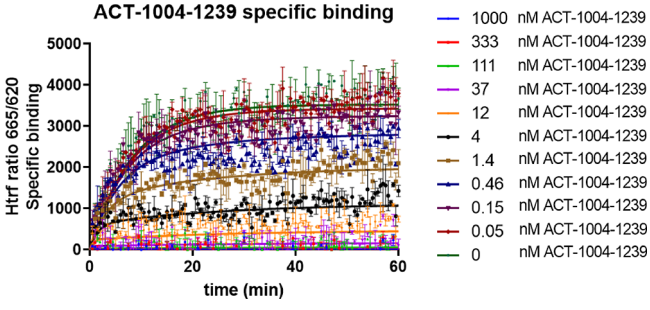

Figure 4. Determination of the K_i, K_{on}, and K_{off} constants (specific binding) of ACT-1004-1239.

concentrations over 24 h in comparison to vehicle-treated mice. These data demonstrate the inhibition of CXCR7-mediated degradation of circulating CXCL12 with ACT-1004-1239. At the highest dose tested (100 mg/kg), a single oral

https://dx.doi.org/10.1021/acs.jmedchem.0c01588
J. Med. Chem. XXXX, XXX, XXX−XXX

Table 10. Pharmacokinetic Parameters of ACT-1004-1239 in Rat and Dog[a]

$AUC_{0\text{-last}}$ (ng/h/mL)	C_{max} (ng/h/mL)	T_{max} (h)	F (%)	$AUC_{0\text{-Inf}}$ (ng/h/mL)	V_{ss} (L/kg)	Cl (mL/min/kg)	$T_{1/2}$ (h)	Cl_{int} (mL/min/mg)	PPB (%)
rat, 10 mg/kg				rat, 1 mg/kg				RLM	rat
827	600	0.5	35	238	3.6	70	1.3	140	91.8
dog, 1 mg/kg				dog, 1 mg/kg				DLM	dog
3620	314	1.5	61	5940	1.6	2.8	6.6	5	83.9

[a]Observed pharmacokinetic parameters are average values for rat, p.o. (n = 3), iv (n = 2), dog p.o./iv (n = 2). T_{max} is given as median. Blood/plasma ratios for rat and dog are 1.1 and 0.7, respectively. Mean conc. 8 h post oral dose was 18.3 ng/mL in the rat and 185 ng/mL in the dog.

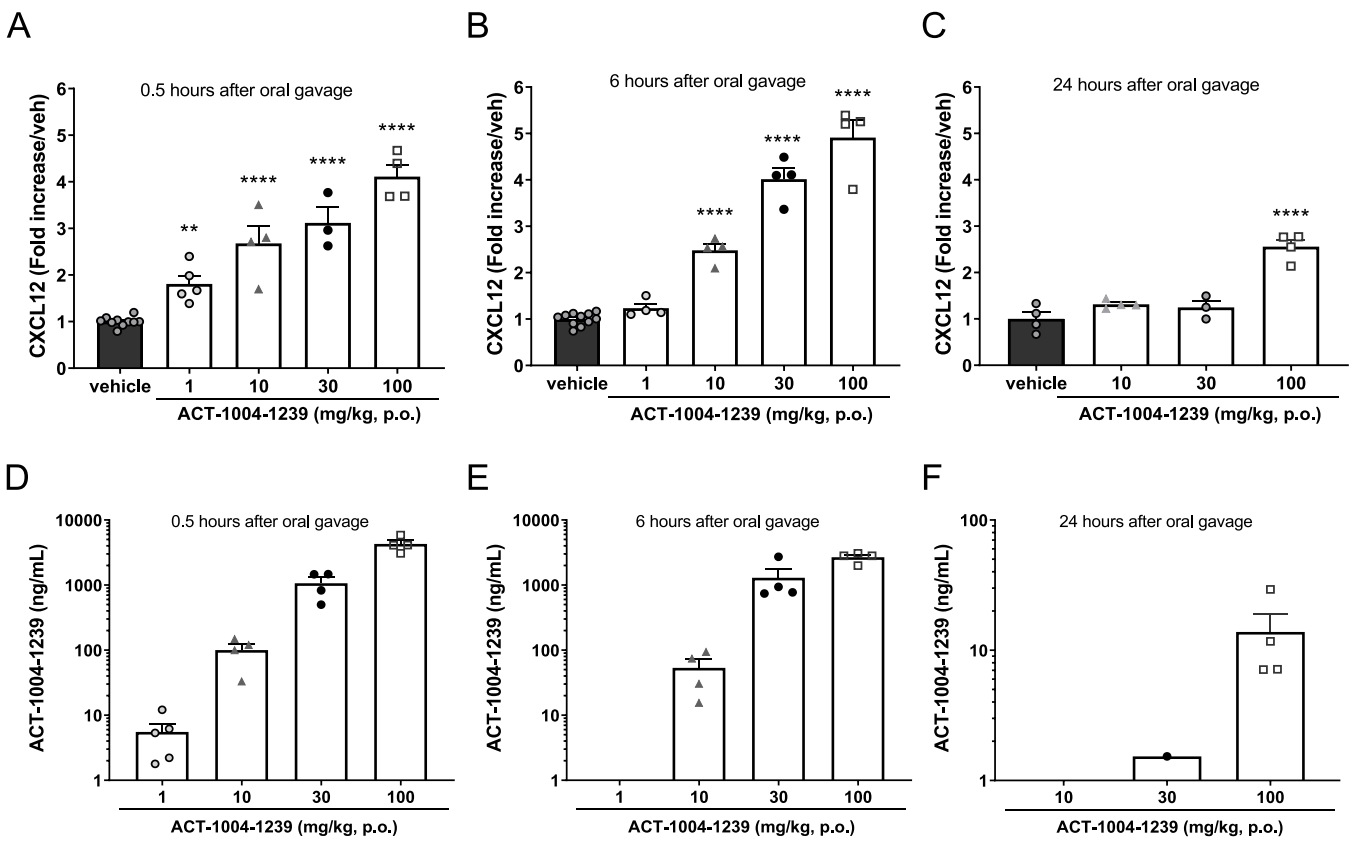

Figure 5. Effect of a single oral administration (p.o.) of ascending doses of ACT-1004-1239 on CXCL12 plasma concentration (upper row) and compound plasma concentration (lower row) in naive male DBA/1 mice. CXCL12 plasma concentration was measured at 0.5 (A), 6 (B), or 24 h (C) after a single oral administration of ACT-1004-1239. Results are expressed as fold change to vehicle-treated mice. ACT-1004-1239 plasma concentration measured 0.5 (D), 6 (E), or 24 h (F) after a single oral administration. Results are expressed as mean + standard error of the mean (SEM) (n = 3−5/dose group). **p < 0.01, ***p < 0.001, ****p < 0.0001 vs vehicle, using one-way analysis of variance (ANOVA) followed by the Dunnett's multiple comparisons test.

dose of ACT-1004-1239 induced a 4.1- to 4.9-fold mean CXCL12 plasma elevation relative to control mice, 0.5 and 6 h after dosing, respectively (Figure 5, panels A and B). The duration of this increase was also dose dependent. At doses up to 30 mg/kg, CXCL12 plasma concentrations returned to vehicle levels within 24 h, whereas with 100 mg/kg of ACT-1004-1239, 24 h after administration, CXCL12 plasma levels were still substantially increased (2.6-fold; p < 0.01 vs vehicle-treated mice) (Figure 5, panel C). Nevertheless, even at this dose, CXCL12 plasma concentrations returned to levels similar to vehicle-treated mice within 96 h post dosing (data not shown). The second ligand of CXCR7, CXCL11, an inducible chemokine was also measured in plasma but did not significantly increase in naïve mice after a single oral dose (data not shown). The plasma concentrations of ACT-1004-1239 increased in a dose-dependent manner and reached a maximum after 0.5 h, with plasma concentrations ranging from 6 ± 2 ng/mL (1 mg/kg single oral dose) to 4285 ± 579 ng/mL (100 mg/kg single oral dose) (Figure 5, panel D). At doses of 30 mg/kg and below, no compound was quantifiable 24 h after oral administration (below the limit of quantification: 1.52 ng/mL) whereas at 100 mg/kg, 14 ± 5 ng/mL of compound was still measured in the plasma (Figure 5, panel F). Based on these results, twice daily oral administration of ACT-1004-1239 might be needed in murine disease models to reach high enough drug plasma concentration at trough, to maintain sustained CXCL12 elevation at all times.

CHEMISTRY

An enantioselective synthesis[41] of *N*-boc-trans-4-aminopiperidine-3-carboxylic acid ethyl ester **15** employing α-methylbenzylamine as a chiral auxiliary and nitrogen source was used to generate both *trans* enantiomers (Scheme 1) and allowed the establishment of the absolute stereochemistry of both

https://dx.doi.org/10.1021/acs.jmedchem.0c01588
J. Med. Chem. XXXX, XXX, XXX−XXX

enantiomers, (3*R*,4*R*)-**11i** and (3*S*,4*S*)-**11i**. This synthetic route further offers the advantage that it can be used to explore stepwise substitution at the three exit vectors of the piperidine scaffold.

4-Oxo-piperidine-1,3-dicarboxylic acid 1-*tert*-butyl ester 3-ethyl ester was reacted with the chiral auxiliary (*S*)-(−)-*α*-methylbenzylamine in refluxing toluene containing a catalytic amount of *p*-toluenesulfonic acid to form enamine **12**. The enamine was reduced with a mixture of $NaBH_4$ and isobutyric acid at 0 °C. The resulting 4:1 mixture of the two *cis*-diastereomers of the *β*-amino ester **13** was treated with sodium ethanolate in ethanol causing epimerization to the *trans*-*β*-aminoester **14**. The pure (*S*,*S*)-*β*-aminoester **14** was isolated from the mixture as the hydrochloride salt in 16% yield. A cleavage of the *α*-methylbenzyl group was achieved with ammonium formiate in the presence of 10% Pd/C in refluxing MeOH. During this reaction, a transesterification to the methyl ester occurred. The *trans* primary amine **15** was acylated with 5-(2,4-difluoro-phenyl)-isoxazole-3-carboxylic acid to deliver the *trans*-(3*S*,4*S*)-4-{[5-(2,4-difluoro-phenyl)-isoxazole-3-carbonyl]-amino}-piperidine-1,3-dicarboxylic acid 1-*tert*-butyl ester 3-methyl ester **16**. N-Boc deprotection with HCl in 1,4-dioxane to the secondary amine **17** followed by *N*-alkylation with cyclohexanone under reductive amination conditions with sodium triacetoxy borohydride in the presence of acetic acid furnished the amine **18**. The ester moiety of **18** was hydrolyzed with NaOH in a THF/water mixture to **19**. HATU-mediated amide bond formation with aq. dimethyl amine was executed in a moderate yield to furnish the dimethyl amide, which after comparison of the chromatogram on chiral stationary phase was found to correspond to the less potent enantiomer (3*S*,4*S*)-**11i**. Repetition of the same sequence of reactions with (*R*)-(+)-*α*-methylbenzylamine as chiral auxiliary delivered the more potent (*R*,*R*)-enantiomer (3*R*,4*R*)-**11i**.

Because of the poor isolated yield of the pure diastereomer hydrochloride **14**, a modified procedure was needed to allow for further structural modifications of the 1-(pyrimidin-2-yl)cyclopropyl amide at 3-position through modification of substituents on *N*-1 by alkylation of the versatile secondary amine (Scheme 2). Our modified synthetic approach toward the (*S*,*S*)-4-aminopiperidine-3-carboxylic ethyl ester followed the strategy we have previously employed in Scheme 1, but equilibration toward the more stable *trans* isomer was done after introduction of the 4-amide. 4-Oxo-piperidine-1,3-dicarboxylic acid 1-*tert*-butyl ester 3-ethyl ester was reacted with the chiral auxiliary (*S*)-(−)-*α*-methylbenzylamine in refluxing toluene containing catalytic amount of *p*-toluenesulfonic acid to form enamine **12**. The enamine was reduced with a mixture of $NaBH_4$ and 3 eq. trifluoracetic acid in THF at −20 °C to give **13**. The 4-*α*-methylbenzylamine was cleaved by hydrogenation with H_2 in the presence of 20% $Pd(OH)_2/C$ in EtOH and the *cis* primary amine **22** was acylated with 5-(2,4-difluoro-phenyl)-isoxazole-3-carboxylic acid to deliver the 6:1 mixture of *cis*-(3*R*,4*S*)-and *cis*-(3*S*,4*R*)-4-{[5-(2,4-difluoro-phenyl)-isoxazole-3-carbonyl]-amino}-piperidine-1,3-dicarboxylic acid 1-*tert*-butyl ester 3-ethyl ester **23**. Treatment with sodium ethanolate in ethanol and ethyl acetate causing epimerization to the *trans*-*β*-aminoesters, followed by chiral chromatography, delivered the pure (3*S*,4*S*)-diastereomer **24**. The ester was hydrolyzed with NaOH in a THF/water mixture. HATU-mediated amide bond formation on **25** with 1-pyrimidin-2-yl-cyclopropylamine delivered the di-amide **26**. N-Boc-deprotection with HCl in 1,4-dioxane gave the piperidine **27**, which was alkylated under reductive amination condition with sodium triacetoxyborohydride in the presence of acetic acid or by reaction with the corresponding alkyl halides in the presence of a base to furnish final compounds **28a**−**28o**.

CONCLUSIONS

In summary, ACT-1004-1239 (compound **28f**) was identified and broadly characterized as a potent, insurmountable, selective, and orally bioavailable antagonist of CXCR7, starting from hits obtained in an innovative HTS assay using an in-house agonist of CXCR7 to allow for a different assay window. The introduction of an additional exit vector in position 3 of the 4-amino-piperidine core led to a breakthrough in terms of potency, binding kinetics, and overall physicochemical and ADMET properties. Further studies demonstrated that modulation of lipophilicity and basicity by combination of substituents on this trisubstituted 4-amino-piperidine scaffold yielded compounds with good CXCR7 antagonism. Compound ACT-1004-1239 demonstrated target engagement *in vivo*. ACT-1004-1239 showed a dose-dependent increase of CXCL12 plasma concentration in mice. Overall, ACT-1004-1239 has favorable ADMET properties. The Cl_{int} measured in HLM is low and with the understanding generated in PK studies in rat and dog; the compound has the potential to be well absorbed and to display a low systemic clearance in humans.

EXPERIMENTAL SECTION

Commercially available starting materials were used as received without further purification. All reactions were carried out in oven-dried glassware under an atmosphere of nitrogen or argon. Flash column chromatography (FC) was performed using RediSEp Rf normal-phase silica flash columns on silica gel (average particle size 0.035−0070 mm) from Teledyne Isco.; elution was performed with EtOAc, heptane, DCM, MeOH, or mixture thereof. Analytical LC−MS data were obtained on a binary gradient pump Agilent G4220A with mass spectrometry detection (single-quadrupole mass analyzer, Thermo Finnigan MSQPlus or equivalent); acidic conditions (Method A): column Zorbax SB-aq (3.5 *μ*m, 4.6 × 50 mm); eluents: A, H_2O + 0.04% TFA. B: MeCN; gradient: 5−95% B over 1.5 min (flow: 4.5 mL/min). Detection: UV/vis + MS or basic conditions (Method B): column Waters BEC C18 (2.5 *μ*m, 3.0 × 50 mm); eluents: A, H_2O + 0.5% NH_4OH (25% aq.); B, MeCN gradient: 5% B to 95% B, over 1.5 min (flow: 1.6 mL/min). Detection: UV/vis + MS. Prep-HPLCs were performed on binary gradient pump Gilson 333/334 or equivalent with mass spectrometry detection (single-quadrupole mass analyzer, Thermo Finnigan MSQPlus or equivalent); XBridge Prep C18 columns from Waters. Eluents: A, H_2O + 0.5% acidic or basic additive (HCO_2H or NH_4OH 25% in H_2O); B, MeCN; gradient 5% B to 95% B over 5 min. Detection: UV/vis and/or MS. Retention time t_R is given in min; molecular weight obtained from the mass spectrum is given in g/mol. Purity of all final compounds was checked by an additional LC−MS analysis (QC LC−MS) on a Waters Acquity UPLC-SQD system equipped with a Waters Acquity binary pump, a Waters SQ Detector, an Acquity UPLC PDA detector; columns: Acquity UPLC CSH C18 1.7 *μ*m, 2.1 mm × 50 mm from Waters, gradient: 2−98% MeCN containing 0.045% formic acid in H_2O containing 0.05% formic acid over 2 min; flow: 1.0 mL/min; 60 °C. According to these LC−MS analyses, final compounds showed a purity of greater than 95% (UV at 214 and at 230 nm). Most compounds were obtained as lyophilizates or dry films. Chiral integrity was proven by HPLC (chiral stationary phase): Hardware from UltiMate instrument series (Dionex): HPG-3200SD binary pump, WPS-3000 autosampler, TCC-3200 thermostated column compartment, DAD-3000 detector, SRD-3400 degasser; ValveMate 2 (Gilson) solvent valves. Chiral integrity was also proven by SFC: CO_2

https://dx.doi.org/10.1021/acs.jmedchem.0c01588
J. Med. Chem. XXXX, XXX, XXX−XXX

supply: Aurora Fusion A5 Evolution; pump: Agilent G4302A; UV detector: Agilent G1315C. Column, solvent, and retention time (t_R) as indicated, flow 1 mL/min. No racemisation/epimerization was observed during the synthesis of the target compounds. Chiral preparative HPLC chromatography were performed with a Varian SD1 pump equipped with a Dionex DAD-3000 UV detector with columns from ChiralPak IA, IB, IC, IE, or IF, 5 μm, 20 × 250 mm, or Regis (*R,R*) Whelk-O1, 21.1 × 250mm, 5 μm; eluent: appropriate mixture of A (0−90% Hept) and B (10−100% EtOH, 0.1% DEA), flow: appropriate flow of 16, 23, or 34 mL/min. Chiral SFC chromatography was performed with: CO_2 supply: Maximator DLE15-GG-C; pumps: 2 SSI HF CP 300; UV detector: Dionex DAD-3000 with columns Regis (*R,R*) Whelk-O1, 30 × 250 mm, 5 μm or ChiralPak IC, 30 × 250 mm, 5 μm; eluent: appropriate mixture of A (60−80% CO_2), and B (30−40% of DCM/EtOH/DEA 50:50:0.1), flow 160 mL/min. LC-HRMS analysis was performed on a Waters Acquity UPLC-SYNAPTG2MS system equipped with a Waters Acquity Binary pump, a SYNAPT G2MS MS Solvent Manager; source temperature: 150 °C, desolvation temperature: 500 °C; desolvation gas flow: 800 L/h; cone gas flow: 20 L/h; extraction cone: 5, RF lens: 0.1 V; sampling cone: 30; capillary: 2.5 kV; high-resolution mode; gain: 1.0; MS function: 0.15 s per scan, 50−1200 amu in full scan, centroid mode. Lock spray: leucine enkephalin 2 ng/mL (556.2771 Da) scan time 0.2 s with interval of 10 s and average of 10 scans; DAD: Acquity UPLC PDA Detector. Column: Acquity UPLC CSH C18 1.7 μm, 2.1 mm × 50 mm from Waters, thermostatted in the Acquity UPLC Column manager at 60 °C. Eluents: H_2O and 0.05% formic acid; B:CH_3CN and 0.05% formic acid. Gradient: 2−98% B over 2.0 min; flow: 1.0 mL/min. Detection: UV 214 nm and MS. ^{1}H and ^{13}C NMR spectra were recorded at rt. with a Bruker Avance II 400 (400 MHz for ^{1}H, 100 MHz for ^{13}C) or a Bruker Avance HD (500 MHz for ^{1}H; 125 MHz for ^{13}C). Chemical shifts (δ) are reported in parts per million (ppm) relative to the deuterated solvent as the internal standard (δ H: $CDCl_3$ 7.26 ppm, d_6-DMSO 2.50 ppm); multiplicities, s = singlet, d = doublet, t = triplet, q = quadruplet, m = multiplet, br = broad signal; coupling constants are given in Hz. X-ray structure analysis: crystals are sensitive to the solvate loss and therefore to the loss of crystallinity. To avoid solvent loss, the crystals were treated, picked, and mounted at low temperature (approx. 243 K) using an inert gas (N_2) device to protect and cool down the crystals. A single crystal (0.112 × 0.036 × 0.020 mm^3) was mounted on a Rigaku-Oxford Diffraction XtaLAB Synergy-S dual source diffractometer equipped with a kappa-axis four-circle goniometer and a Dectris Pilatus3 R 200 K HPC (Hybrid Photon Counting) detector and Cu and Mo PhotonJet microfocus X-ray sources. Reflections were collected at 253 K using monochromatic Cu Kα radiation. For the structure solution, the program SHELXT[42] implemented in the APEX-III Bruker AXS, V.2018.7-2 software was used. The structure refinement was done with SHELXL[43] as implemented in APEX-III software. Full matrix least-squares refinement was performed with anisotropic temperature factors for all the nondisordered atoms. The disordered part (see Supporting Information for details) was refined with isotropic temperature factors to achieve stability of the refinement cycles and avoid the introduction of constrains in the molecule. The solvate molecule present (MeOH) is disordered over at least 3 positions. Due to the "not so good" data quality, the solvate positions cannot be fully refined, nor found completely. Therefore, to avoid such problems and instability of the refinement, the MeOH solvate was SQUEEZED out using the program Platon[44] Squeeze. Most of the hydrogen atoms present were fixed in the refinement, the two hydrogen atoms involved in donor-acceptor hydrogen bonds were refined freely. Coordinates, anisotropic temperature factors, bond lengths, angles, and special refinement issues are deposited with the Cambridge Crystallographic Data Centre, CCDC 1993933.

(3*S*,4*S*)-4-Amino-piperidine-1,3-dicarboxylic Acid 1-*tert*-Butyl Ester 3-Methyl Ester (15). A solution of (3*S*,4*S*)-4-((*S*)-1-phenyl-ethylamino)-piperidine-1,3-dicarboxylic acid 1-*tert*-butyl ester 3-ethyl ester **14**[41] (2.41 g, 6.66 mmol) in MeOH (10 mL) was added to a suspension of palladium on activated charcoal (10%) (250 mg) and ammonium formate (3.35 g, 53.28 mmol) in MeOH (60 mL) under N_2. The mixture was refluxed for 6 h. After the reaction was complete (disappearance of the starting material but also exchange of the ethyl− for the methyl ester), the cooled solution was filtered through Celite and the filtrate was concentrated to obtain the title product (1.48 g, 86%) as a slightly yellow oil. LC−MS method A: t_R = 0.53 min; $[M + H]^+$ = 259.23. ^{1}H NMR (400 MHz, $CDCl_3$) δ: 4.32−4.58 (m, 1H), 4.16−4.25 (m, 1H), 3.77 (s, 3H), 3.41 (td, J_1 = 11.2 Hz, J_2 = 4.1 Hz, 1H), 2.67−2.89 (m, 3H), 2.10 (dd, J_1 = 13.1 Hz, J_2 = 3.5 Hz, 1H), 1.64 (m, 1H), 1.48 (m, 11H).

(3*S*,4*S*)-4-{[5-(2,4-Difluoro-phenyl)-isoxazole-3-carbonyl]-amino}-piperidine-1,3-dicarboxylic Acid 1-*tert*-Butyl Ester 3-Methyl Ester (16). To a solution of (3*S*,4*S*)-4-amino-piperidine-1,3-dicarboxylic acid 1-*tert*-butyl ester 3-methyl ester **15** (1.463 g, 5.37 mmol) in DMF (17 mL) at rt. was added 5-(2,4-difluorophenyl)-isoxazole-3-carboxylic acid (1.21 g, 5.37 mmol). DIPEA (2.3 mL, 13.34 mmol) was then added followed by HATU (2.451 g, 6.44 mmol). The reaction mixture was stirred overnight at rt. The reaction mixture was concentrated, dissolved in DCM (100 mL), and washed twice with aq. sat. $NaHCO_3$ (2 × 100 mL). The organic layer was dried over $MgSO_4$ and evaporated. The crude residue was purified by flash chromatography over 40 g of silica gel with heptane/EtOAc (1:0 to 3:1) as eluent to yield **16** (2.38 g, 95%) as a white powder; LC−MS method A: t_R = 0.94 min; $[M + H]^+$ = 466.04. ^{1}H NMR (400 MHz, D_6-DMSO) δ: 8.90 (d, J = 8.8 Hz, 1H), 8.06 (td, J_1 = 6.5 Hz, J_2 = 8.7 Hz, 1H), 7.58 (m, 1H), 7.33 (td, J_1 = 2.3 Hz, J_2 = 8.4 Hz, 1H), 7.13 (d, J = 2.9 Hz, 1H), 4.26 (m, 1H), 4.04−4.10 (m, 1H), 3.94 (d, J = 11.8 Hz, 1H), 3.56 (s, 3H), 2.86−3.04 (m, 2H), 2.66 (td, J_1 = 11.0 Hz, J_2 = 4.1 Hz, 1H), 1.80 (dd, J_1 = 13.6 Hz, J_2 = 4.5 Hz, 1H), 1.53 (m, 1H), 1.42 (m, 9H).

(3*S*,4*S*)-4-{[5-(2,4-Difluoro-phenyl)-isoxazole-3-carbonyl]-amino}-piperidine-3-carboxylic Acid Methyl Ester Hydrochloride (17). (3*S*,4*S*)-4-{[5-(2,4-Difluoro-phenyl)-isoxazole-3-carbonyl]-amino}-piperidine-1,3-dicarboxylic acid 1-*tert*-butyl ester 3-methyl ester **16** (1.13 g, 2.42 mmol) was dissolved in MeOH (12 mL). HCl in dioxane 4 M (12 mL, 48 mmol) was added dropwise. The mixture was stirred at rt. for 1 h. The solvents were evaporated, and the residue was dried on HV to deliver the title crude compound **17**, (0.97 g, quantitative) as a white powder. LC−MS method A: t_R = 0.61 min; $[M + H]^+$ = 366.18. ^{1}H NMR (400 MHz, D_6-DMSO) δ: 9.21 (d, J = 8.6 Hz, 1H), 9.09−9.10 (m, 1H), 8.08 (m, 1H), 7.60 (m, 1H), 7.35 (td, J_1 = 2.2 Hz, J_2 = 8.6 Hz, 1H), 7.19 (d, J = 2.9 Hz, 1H), 4.34 (m, 1H), 3.58 (s, 5H), 3.47−3.50 (m, 1H), 3.14 (dd, J_1 = 0.9 Hz, J_2 = 2.4 Hz, 2H), 3.03 (m, 1H), 1.97 (d, J = 2.9 Hz, 2H).

(3*S*,4*S*)-1-Cyclohexyl-4-{[5-(2,4-difluoro-phenyl)-isoxazole-3-carbonyl]-amino}-piperidine-3-carboxylic Acid Methyl Ester (18). To a suspension of (3*S*,4*S*)-4-{[5-(2,4-difluoro-phenyl)-isoxazole-3-carbonyl]-amino}-piperidine-3-carboxylic acid methyl ester hydrochloride **17** (0.95 g, 2.36 mmol) in DCM (20 mL) at rt. was added cyclohexanone (0.57 mL, 5.47 mmol) followed by acetic acid (0.35 mL, 6.13 mmol) and sodium triacetoxyborohydride (1.23 g, 5.93 mmol). The reaction mixture was stirred overnight at rt. The reaction mixture was diluted with DCM (30 mL) and washed twice with aq. sat. $NaHCO_3$ (2 × 50 mL). The organic phase was dried over $MgSO_4$ and evaporated. Purification by flash chromatography over 40 g of silica gel with heptane/EtOAc (1:0 to 0:1) as eluent yielded **18**, (1.00 g, 95%) as an off-white solid. LC−MS method A: t_R = 0.71 min; $[M + H]^+$ = 448.17. ^{1}H NMR (400 MHz, D_6-DMSO) δ: 8.87−8.92 (m, 1H), 8.06 (q, J = 7.7 Hz, 1H), 7.59 (t, J = 10.2 Hz, 1H), 7.34 (t, J = 8.5 Hz, 1H), 7.13 (s, 1H), 3.96−4.10 (m, 1H), 3.54 (s, 3H), 2.96−3.07 (m, 1H), 2.68−2.89 (m, 2H), 2.34−2.42 (m, 3H), 1.73−1.81 (m, 5H), 1.56−1.64 (m, 2H), 1.14−1.20 (m, 4H), 1.04−1.10 (m, 1H).

(3*S*,4*S*)-1-Cyclohexyl-4-{[5-(2,4-difluoro-phenyl)-isoxazole-3-carbonyl]-amino}-piperidine-3-carboxylic Acid Hydrochloride (19). (3*S*,4*S*)-1-Cyclohexyl-4-{[5-(2,4-difluoro-phenyl)-isoxazole-3-carbonyl]-amino}-piperidine-3-carboxylic acid methyl ester **18** (0.95 g, 2.11 mmol) was dissolved in THF (14 mL), and 1 M aq. LiOH solution (5.27 mL, 5.27 mmol) was added. The mixture was stirred overnight at rt., 1 M aq. HCl solution (5.27 mL, 5.27 mmol) was added, and the reaction was stirred for 5 min. THF was

https://dx.doi.org/10.1021/acs.jmedchem.0c01588
J. Med. Chem. XXXX, XXX, XXX−XXX

evaporated and the product **19** precipitated. The resulting white solid was filtered off and dried *in vacuo* to yield **19**, (0.788 g, 86%) as a white powder. LC−MS method A: t_R = 0.66 min; $[M + H]^+$ = 434.06. ^{1}H NMR (400 MHz, D_6-DMSO) δ: 12.86 (d, 1H), 10.36−10.38 (m, 1H), 9.24 (d, J = 8.2 Hz, 1H), 8.07 (q, J = 7.8 Hz, 1H), 7.60 (t, J = 10.4 Hz, 1H), 7.35 (t, J = 8.4 Hz, 1H), 7.19 (s, 1H), 4.36 (d, J = 7.5 Hz, 1H), 3.60 (d, J = 8.0 Hz, 1H), 3.42 (m, 1H), 3.18−3.26 (m, 4H), 2.07−2.12 (m, 3H), 2.02 (m, 1H), 1.82 (d, J = 11.8 Hz, 2H), 1.61 (m, 1H), 1.43 (q, J = 11.3 Hz, 2H), 1.26 (q, J = 12.2 Hz, 2H), 1.12 (td, J = 12.8 Hz, 1H).

(3*S*,4*S*)-1-Cyclohexyl-4-{[5-(2,4-difluoro-phenyl)-isoxazole-3-carbonyl]-amino}-piperidine-3-carboxylic Acid Dimethylamide ((3*S*,4*S*)-11i). To a solution of (3*S*,4*S*)-1-cyclohexyl-4-{[5-(2,4-difluoro-phenyl)-isoxazole-3-carbonyl]-amino}-piperidine-3-carboxylic acid hydrochloride **19** (0.102 g, 0.23 mmol) in DMF (5 mL) was added dimethylamine 2 M in THF (0.177 mL, 0.35 mmol). DIPEA (0.13 mL, 0.75 mmol) was then added followed by HATU (0.144 g, 0.38 mmol). The reaction mixture was stirred overnight at rt. The crude mixture was directly purified by prep. HPLC to yield (3*S*,4*S*)-**11i** (0.040 g, 37%) as a white powder. LC−MS method A: t_R = 0.71 min; $[M + H]^+$ = 461.22. Chiral HPLC: t_R = 6.8 min; 99% *ee*; column: Regis (*R*,*R*) Whelk-O1, 4.6 × 250 mm, 5 μm; Detector wavelength: 254 nm; Eluent: 30% heptane 0.05% DEA; 70% ethanol 0.05% DEA; flow: 0.8 mL/min; BPR: 150 bar; temperature: 25 °C. Injection volume: 2.5 μL. LC-HRMS: t_R = 0.59 min; m/z = 460.2285, found = 461.2373 $[M + H]^+$. ^{1}H NMR (500 MHz, D_6-DMSO) δ: 8.69 (d, J = 8.6 Hz, 1H), 8.05 (td, J_1 = 8.7 Hz, J_2 = 6.4 Hz, 1H), 7.58 (m, 1H), 7.33 (m, J_1 = 8.1 Hz, J_2 = 2.0 Hz, 1H), 7.09 (d, J = 2.9 Hz, 1H), 4.08 (m, 1H), 3.13 (td, J_1 = 10.7 Hz, J_2 = 3.6 Hz, 1H), 3.06 (s, 3H), 2.82−2.88 (m, 2H), 2.77 (s, 3H), 2.24−2.32 (m, 2H), 2.19 (t, J = 11.3 Hz, 1H), 1.81−1.85 (m, 1H), 1.73 (d, J = 8.0 Hz, 4H), 1.58 (m, 2H), 1.19 (m, 4H), 1.05−1.09 (m, 1H).

(3*R*,4*S*)-4-((*S*)-1-Phenyl-ethylamino)-piperidine-1,3-dicarboxylic Acid 1-*tert*-Butyl Ester 3-Ethyl Ester (13). Sodium borohydride (1.43 g, 37.85 mmol) was dissolved in THF (100 mL) at −15 °C under N_2. TFA (10.7 mL, 0.14 mmol) was added dropwise over 20 min. 4-((*S*)-1-Phenyl-ethylamino)-5,6-dihydro-2*H*-pyridine-1,3-dicarboxylic acid 1-*tert*-butyl ester 3-ethyl ester[41] **12** (10.5 g, 28 mmol) was added over 10 min at −14 to −18 °C. The resulting mixture was stirred for 60 min at 0 °C. Iced water (100 mL) was added carefully, and the reaction mixture was stirred for 10 min at rt. A 3 M aq. NaOH solution was added to bring the mixture to pH 11. The reaction mixture was extracted with DCM (2 × 100 mL), the combined organic layers were washed with brine (2 × 100 mL) and dried over $MgSO_4$, and the solvent was evaporated under reduced pressure. The resulting oil was purified by flash chromatography over 120 g of silica gel with heptane/EtOAc (1:0 to 4:1) as eluent to give the title product **13** as a yellowish oil, (9.6 g, 91%). The title compound was contaminated by ∼10% of the corresponding (3*S*,4*R*)-isomer. LC−MS method A: t_R = 0.71 min; $[M + H]^+$ = 377.33. ^{1}H NMR (400 MHz, $CDCl_3$) δ: 7.32−7.35 (m, 4H), 7.29−7.30 (m, 1H), 7.24 (m, 1H), 4.19 (q, J = 7.3 Hz, 2H), 4.00 (d, J = 9.2 Hz, 1H), 3.88 (q, J = 6.8 Hz, 1H), 3.69−3.76 (m, 1H), 3.19 (dd, J_1 = 13.8 Hz, J_2 = 3.9 Hz, 1H), 3.01 (m, 1H), 2.87 (m, 1H), 2.79 (s, 1H), 1.81 (s, 1H), 1.76 (m, 1H), 1.51 (m, 1H), 1.44 (m, 9H), 1.28−1.33 (m, 5H).

(3*R*,4*S*)-4-Amino-piperidine-1,3-dicarboxylic Acid 1-*tert*-Butyl Ester 3-Ethyl Ester (22). A solution of (3*R*,4*S*)-4-((*S*)-1-phenyl-ethylamino)-piperidine-1,3-dicarboxylic acid 1-*tert*-butyl ester 3-ethyl ester **13** (9.6 g, 25.5 mmol) in MeOH (250 mL) was added to a suspension of $Pd(OH)_2$/C 20% (1 g) under H_2. The mixture was stirred for 18 h at rt. The suspension was filtered through Celite, and the filtrate is concentrated under *vacuo* to obtain the title product as a slightly yellow oil **22**, (6.94 g. quantitative). The title compound contained ∼10% of the corresponding (3*S*,4*R*)-isomer. LC−MS method A: t_R = 0.54 min; $[M + H]^+$ = 273.26. ^{1}H NMR (400 MHz, D_6-DMSO) δ: 4.07 (q, J = 7.0 Hz, 2H), 3.28−3.36 (m, 5H), 2.57−2.61 (m, 1H), 1.54−1.68 (m, 2H), 1.34−1.41 (m, 11 H), 1.20 (t, J = 7.3 Hz, 3H).

(3*R*,4*S*)-4-{[5-(2,4-Difluoro-phenyl)-isoxazole-3-carbonyl]-amino}-piperidine-1,3-dicarboxylic Acid 1-*tert*-Butyl Ester 3-Ethyl Ester (23). To a solution of (3*R*,4*S*)-4-amino-piperidine-1,3-dicarboxylic acid 1-*tert*-butyl ester 3-ethyl ester **22** (7.44 g, 27.2 mmol) in DCM (200 mL) at rt. was added 5-(2,4-difluorophenyl)-isoxazole-3-carboxylic acid (6.12 g, 27.3 mmol). TEA (15.2 mL, 109 mmol) was then added followed by T_3P 50% in DCM (32.4 mL, 54.4 mmol). The reaction mixture was stirred for 24 h at rt. The reaction mixture was washed twice with sat. aq. $NaHCO_3$ (2 × 100 mL). The organic layer was dried over $MgSO_4$ and evaporated. The crude residue was purified by flash chromatography over 100 g of silica gel with heptane/EtOAc (1:0 to 85:15) as eluent to yield the title compound **23**, as a white powder (10.25 g, 79%). The title compound contains ∼10% of the corresponding (3*S*,4*R*)-isomer; LC−MS method A: t_R = 1.15 min; $[M + H]^+$ = 480.1. ^{1}H NMR (400 MHz, $CDCl_3$) δ: 8.92 (d, J = 8.9 Hz, 1H), 8.06 (m, 1H), 7.60 (ddd, J_1 = 11.5 Hz, J_2 = 9.3 Hz, J_3 = 2.5 Hz, 1H), 7.33 (td, J_1 = 8.4 Hz, J_2 = 2.2 Hz, 1H), 7.13 (d, J = 2.9 Hz, 1H), 4.35−4.47 (m, 1H), 3.96−4.11 (m, 3H), 3.63−3.82 (m, 1H), 3.38−3.44 (m, 1H), 3.06−3.16 (m, 1H), 2.97−3.01 (m, 1H), 1.90−1.99 (m, 1H), 1.65−1.72 (m, 1H), 1.40 (s, 9H), 1.16 (t, J = 6.9 Hz, 3H).

(3*S*,4*S*)-4-{[5-(2,4-Difluoro-phenyl)-isoxazole-3-carbonyl]-amino}-piperidine-1,3-dicarboxylic Acid 1-*tert*-Butyl Ester 3-Ethyl Ester (24). Sodium ethoxide 95% (4.086 g, 57 mmol) was added portion wise to a solution of (3*R*,4*S*)-4-{[5-(2,4-difluoro-phenyl)-isoxazole-3-carbonyl]-amino}-piperidine-1,3-dicarboxylic acid 1-*tert*-butyl ester 3-ethyl ester **23** (6.837 g, 14.3 mmol) in a mixture of EtOH (80 mL) and EtOAc (40 mL). The mixture was stirred at rt. for 1 day. Sat. aq. NH_4Cl (50 mL) was added to the reaction mixture. EtOH and EtOAc were evaporated at reduced pressure. DCM (150 mL) was added. The organic phase was separated, and the aq. layer extracted thrice with DCM (3 × 100 mL). The combined organic layers were dried over $MgSO_4$, filtered, and concentrated. The crude residue was purified by prep-HPLC with basic conditions. The title compound was obtained as a colorless powder (5.04 g, 74%), containing ∼10% of the corresponding (3*S*,4*R*)-isomer. The enantiomerically pure title compound was obtained by chiral preparative SFC of the mixture of (3*S*,4*S*)-4-{[5-(2,4-difluoro-phenyl)-isoxazole-3-carbonyl]-amino}-piperidine-1,3-dicarboxylic acid 1-*tert*-butyl ester 3-ethyl ester containing ∼10% of (3*R*,4*R*)-4-{[5-(2,4-difluoro-phenyl)-isoxazole-3-carbonyl]-amino}-piperidine-1,3-dicarboxylic acid 1-*tert*-butyl ester 3-ethyl ester using a column ChiralPak IC, 5 μm, 30 × 250 mm; with a mixture of A (80% CO_2) and B (20%: DCM (50%), MeOH (50%), 0.1% DEA) as eluent and a flow of 160 mL/min.; BPR: 100 bar; temperature = 40 °C to deliver **24** (4.32 g, 63%) as a light yellow powder. Chiral SFC HPLC: t_R = 3.24 min; 99% *ee*; column: ChiralPak IC 4.6 × 250 mm, 5 μm; detector wavelength: 254 nm; eluent A (80% CO_2) and eluent B (20%: DCM (50%), MeOH (50%), 0.1% DEA) and a flow of 4.0 mL/min.; BPR: 150 bar; temperature = 40 °C; Flow: 0.8 mL/min; BPR: 150 bar; temperature: 25 °C. Injection volume: 4 μL. LC−MS method A: t_R = 1.06 min; $[M + H]^+$ = 480.08. ^{1}H NMR (D_6-DMSO) δ: 8.93 (d, J = 8.9 Hz, 1H), 8.05−8.10 (m, 1H), 7.59 (ddd, J_1 = 11.5 Hz, J_2 = 9.5 Hz, J_3 = 2.3 Hz, 1H), 7.34 (td, J_1 = 8.4 Hz, J_2 = 2.2 Hz, 1H), 7.14 (d, J = 2.9 Hz, 1H), 4.23−4.32 (m, 1H), 4.03 (q, J = 7.1 Hz, 3H), 3.90−3.98 (m, 1H), 2.82−3.03 (m, 2H), 2.59−2.61 (m, 1H), 1.77−1.81 (m, 1H), 1.48−1.59 (m, 1H), 1.43 (s, 9H), 1.08 (t, J = 7.1 Hz, 3H).

(3*S*,4*S*)-4-{[5-(2,4-Difluoro-phenyl)-isoxazole-3-carbonyl]-amino}-piperidine-1,3-dicarboxylic Acid 1-*tert*-Butyl Ester (25). (3*S*,4*S*)-4-{[5-(2,4-Difluoro-phenyl)-isoxazole-3-carbonyl]-amino}-piperidine-1,3-dicarboxylic acid 1-*tert*-butyl ester 3-ethyl ester **24** (4.98 g, 10.7 mmol) was dissolved in THF (80 mL). Aq. 1 M NaOH solution (20 mL, 20 mmol) was added, and the mixture stirred at rt. for 3 h. The reaction mixture was acidified to around pH = 3 with 2 M aq. HCl solution (10 mL) and extracted thrice with DCM (3 × 50 mL). The combined organic phases were dried over $MgSO_4$, filtered, and concentrated. The title compound **25** was obtained as a white powder (4.73 g, 98%); LC−MS method A: t_R = 0.99 min; $[M + H]^+$ = 452.33. ^{1}H NMR (500 MHz, D_6-DMSO) δ: 12.51 (s, 1H), 8.06 (td, J_1 = 8.7 Hz, J_2 = 6.4 Hz, 1H), 7.59 (m, 1H), 7.34 (td, J_1 = 8.4 Hz, J_2 = 2.3 Hz, 1H), 7.14 (d, J = 2.9 Hz, 1H), 4.25

https://dx.doi.org/10.1021/acs.jmedchem.0c01588
J. Med. Chem. XXXX, XXX, XXX−XXX

(m, 1H), 4.05−4.16 (m, 1H), 3.92−3.94 (m, 1H), 2.79−3.00 (m, 2H), 2.59 (td, J_1 = 11.0 Hz, J_2 = 4.1 Hz, 1H), 1.78−1.82 (m, 1H), 1.49 (m, 2H), 1.42 (m, 9H).

(3*S*,4*S*)-4-{[5-(2,4-Difluoro-phenyl)-isoxazole-3-carbonyl]-amino}-3-(1-pyrimidin-2-yl-cyclopropylcarbamoyl)-piperidine-1-carboxylic Acid *tert*-Butyl Ester (26). To a solution of (3*S*,4*S*)-4-{[5-(2,4-difluoro-phenyl)-isoxazole-3-carbonyl]-amino}-piperidine-1,3-dicarboxylic acid 1-*tert*-butyl ester **25** (2.5 g, 5.54 mmol) in DMF (25 mL) were added 1-(pyrimidin-2-yl)cyclopropan-1-amine hydrochloride (0.97 g, 5.54 mmol), DIPEA (2.37 mL, 13.8 mmol), and HATU (2.527 g, 6.65 mmol). The reaction mixture was stirred at rt. for 4 h. The volatiles were evaporated, and the crude mixture purified by flash chromatography over 40 g of silica gel with heptane/EtOAc (1:1 to 0:1) as eluent to yield **26** as a white powder (2.74 g, 87%); LC−MS method A: t_R = 0.95 min; $[M + H]^+$ = 568.97. ^{1}H NMR (400 MHz, D_6-DMSO) δ: 8.63 (d, J = 8.6 Hz, 1H), 8.53 (d, J = 4.9 Hz, 3H), 8.08 (td, J_1 = 8.7 Hz, J_2 = 6.4 Hz, 1H), 7.57 (ddd, J_1 = 11.5 Hz, J_2 = 9.3 Hz, J_3 = 2.5 Hz, 1H), 7.34 (td, J_1 = 8.2 Hz, J_2 = 2.1 Hz, 1H), 7.19 (t, J = 4.9 Hz, 1H), 7.17 (d, J = 3.0 Hz, 1H), 4.12−4.25 (m, 2H), 3.96−3.99 (m, 1H), 2.77−2.99 (m, 2H), 2.58 (td, J_1 = 11.2 Hz, J_2 = 4.0 Hz, 1H) 1.82−1.86 (m, 1H), 1.44−1.53 (m, 11 H), 1.35−1.39 (m, 1H), 1.03−1.13 (m, 2H).

(3*S*,4*S*)-4-{[5-(2,4-Difluoro-phenyl)-isoxazole-3-carbonyl]-amino}-piperidine-3-carboxylic Acid (1-Pyrimidin-2-yl-cyclopropyl)-amide Hydrochloride (27). (3*S*,4*S*)-4-{[5-(2,4-Difluoro-phenyl)-isoxazole-3-carbonyl]-amino}-3-(1-pyrimidin-2-yl-cyclopropylcarbamoyl)-piperidine-1-carboxylic acid *tert*-butyl ester **26** (1.81 g, 3.18 mmol) was dissolved in dioxane (10 mL). HCl in dioxane 4 M (4 mL, 16 mmol) was added dropwise. The mixture was stirred at rt. for 1 h. The solvents were evaporated, and the residue dried in HV to deliver crude **27** as a white powder (1.57 g, 98%). LC−MS method A: t_R = 0.64 min; $[M + H]^+$ = 469.17. ^{1}H NMR (400 MHz, D_6-DMSO) δ: 8.54 (d, J = 8.2 Hz, 1H), 8.50 (d, J = 4.8 Hz, 2H), 8.41 (s, 1H), 8.07 (q, J = 8.8 Hz, 1H), 7.59 (m, 1H), 7.33 (td, J_1 = 8.5 Hz, J_2 = 1.6 Hz, 1H), 7.18 (m, 2H), 4.03−4.11 (m, 1H), 3.11 (d, J = 9.5 Hz, 1H), 2.96 (d, J = 11.9 Hz, 1H), 2.59 (m, 2H), 1.81 (d, J = 9.5 Hz, 1H), 1.35−1.50 (m, 4H), 1.24 (m, 1H), 1.04−1.14 (m, 3H).

(3*S*,4*S*)-1-Cyclopropylmethyl-4-{[5-(2,4-difluoro-phenyl)-isoxazole-3-carbonyl]-amino}-piperidine-3-carboxylic Acid (1-Pyrimidin-2-yl-cyclopropyl)-amide (28f). To a suspension of (3*S*,4*S*)-4-{[5-(2,4-difluoro-phenyl)-isoxazole-3-carbonyl]-amino}-piperidine-3-carboxylic acid methyl ester hydrochloride **27** (0.200 g, 0.396 mmol) in DCM (20 mL) at rt. was added cyclopropanecarboxaldehyde (0.03 mL, 0.396 mmol) followed by DIPEA (0.2 mL, 1.2 mmol) and sodium triacetoxyborohydride (0.221 g, 1 mmol). The reaction mixture was stirred for 2 h at rt. The reaction mixture was washed twice with aq. sat. $NaHCO_3$ (2 × 50 mL). The organic phase was dried over $MgSO_4$ and evaporated. The crude residue was purified by prep. HPLC under basic conditions to yield **28f** (0.148 g, 72%) as a colorless solid, which can be crystallized from MeCN or MeCN/H_2O. LC−MS method A: t_R = 0.69 min; $[M + H]^+$ = 523.04. Chiral HPLC: t_R = 7.0 min; >99% *ee*; column: ChiralPak IC 4.6 × 250 mm, 5 μm; Detector wavelength: 254 nm; eluent: 10% heptane 0.05% DEA; 90% ethanol 0.05% DEA; Flow: 1.2 mL/min; BPR: 150 bar; temperature: 25 °C. Injection volume: 2 μL. LC-HRMS: t_R = 0.57 min; m/z = 522.2191, found = 523.2265 $[M + H]^+$. ^{1}H NMR (500 MHz, D_6-DMSO) δ: 8.54 (d, J = 8.5 Hz, 1H), 8.51 (d, J = 4.8 Hz, 2H), 8.45 (s, 1H), 8.08 (td, 1H), 7.59 (ddd, J_1 = 11.4 Hz, J_2 = 9.4 Hz, J_3 = 2.4 Hz, 1H), 7.34 (td, J_1 = 2.1 Hz, J_2 = 8.4 Hz, 1H), 7.18 (t, J = 4.8 Hz, 1H), 7.16 (d, J = 2.9 Hz, 1H), 3.99 (m, 1H), 3.14 (d, J = 9.5 Hz, 1H), 2.99 (d, J = 11.3 Hz, 1H), 2.72 (td, J_1 = 3.6 Hz, J_2 = 11.0 Hz, 1H), 2.23 (m, 2H), 2.12 (t, J = 11.4 Hz, 1H), 2.01 (t, J = 10.5 Hz 1H), 1.84−1.87 (d, J = 8.7 Hz 1H), 1.62 (m, 1H), 1.48−1.51 (m, 1H), 1.35−1.39 (m, 1H), 1.05−1.12 (m, 2H), 0.83−0.88 (m, 1H), 0.47−0.50 (m, 2H), 0.10 (m, 2H). ^{13}C NMR (125 MHz, D_6-DMSO) δ: 172.5 (s), 170.2 (s), 164.2 (dd, J_1 = 252 Hz, J_2 = 13 Hz), 160.2 (s), 159.4 (dd, J_1 = 256 Hz, J_2 = 13 Hz), 157.8 (s), 157.3 (s), 130.2 (dd, J_1 = 3 Hz, J_2 = 10 Hz), 118.7 (s), 113.5 (dd, J_1 = 3 Hz, J_2 = 22 Hz), 111.9 (dd, J_1 = 4 Hz, J_2 = 12 Hz), 106.0 (t, J = 26 Hz), 103.0 (d, J = 8 Hz), 63.0 (s), 55.7 (s), 52.5 (s), 49.2 (s), 47.8 (s), 36.5 (s), 31.5 (s), 19.5 (d, J = 17 Hz), 9.0 (s), 4.3 (d, J = 12 Hz).

■ ASSOCIATED CONTENT

Supporting Information

The Supporting Information is available free of charge at https://pubs.acs.org/doi/10.1021/acs.jmedchem.0c01588.

Detailed experimental procedures and analytical data of HTS hits **2**−**6**; synthesized compounds **7a**−**31** and respective precursors; X-ray crystallographic structure parameters of compound **28f**; method for the determination of the melting point by differential scanning calorimetry (DSC); method for the determination of log $D_{7.4}$ and pK_a values; method describing the CXCR7-agonist **1** assay, including insurmountability determination; method describing the CXCR7-CXCL12 assay; experimental details for the biological assays to assess the potency of **28f** on CXCR7 from various species, on human CXCR4 and to determine its K_i, K_{on}, and K_{off} constants; and experimental details for the cytochrome P450 enzyme inhibition assays, for the metabolic stability studies, the detailed description of the pharmacokinetic studies in rat and dog, and the target engagement *in vivo* (PDF)

Molecular formula strings (CSV)

Accession Codes

The corresponding data set has been deposited at the Cambridge Crystallographic Data Centre, 12 Union Road, Cambridge CB2 1EZ, United Kingdom, http://www.ccdc.cam.c.uk/, under the following deposition number: CCDC 1993933 (compound **28f**, see the Supporting Information).

■ AUTHOR INFORMATION

Corresponding Authors

Sylvia Richard-Bildstein − *Drug Discovery, Idorsia Pharmaceuticals Ltd., Allschwil CH-4123, Switzerland;* orcid.org/0000-0001-6588-1599; Phone: +41-58-844-06-87; Email: sylvia.richard@idorsia.com

Philippe Guerry − *Drug Discovery, Idorsia Pharmaceuticals Ltd., Allschwil CH-4123, Switzerland;* orcid.org/0000-0001-5631-1279; Phone: +41-58-844-02-88; Email: philippe.guerry@idorsia.com

Authors

Hamed Aissaoui − *Drug Discovery, Idorsia Pharmaceuticals Ltd., Allschwil CH-4123, Switzerland*

Julien Pothier − *Drug Discovery, Idorsia Pharmaceuticals Ltd., Allschwil CH-4123, Switzerland*

Gabriel Schäfer − *Drug Discovery, Idorsia Pharmaceuticals Ltd., Allschwil CH-4123, Switzerland;* orcid.org/0000-0002-7792-9542

Carmela Gnerre − *Drug Discovery, Idorsia Pharmaceuticals Ltd., Allschwil CH-4123, Switzerland*

Eleanor Lindenberg − *Drug Discovery, Idorsia Pharmaceuticals Ltd., Allschwil CH-4123, Switzerland*

François Lehembre − *Drug Discovery, Idorsia Pharmaceuticals Ltd., Allschwil CH-4123, Switzerland*

Laetitia Pouzol − *Drug Discovery, Idorsia Pharmaceuticals Ltd., Allschwil CH-4123, Switzerland*

Complete contact information is available at: https://pubs.acs.org/10.1021/acs.jmedchem.0c01588

Author Contributions

The manuscript was written through contributions of all authors. All authors have given approval to the final version of the manuscript.

Funding

No funding was provided.

Notes

The authors declare no competing financial interest.

■ ACKNOWLEDGMENTS

We thank Dr. Eric A. Ertel and Dr. Martin Holdener for helpful discussions, Viktor Ribic, Siefke Siefken, Clément Popineau, Pascal Rebmann, Audrey Izard, Aurelien Mérot, Philippe Risch, Mélanie Garnier, Ann Natalie de Leon for the synthesis and characterization of the compounds, Julien Grimont, François Le Goff and Marco Caldarone for the analysis of the compounds, Benedicte Haenig, Panja Strickner and Manon Kiry for performing the biological assays, Romain Sube, Camille Forni and Cédric Etien for hERG blockage measurements, the DMPK as well as the preformulation and preclinical galenics groups for their continuous support with routine *in vitro* and *in vivo* experiments, Anna Sassi, Nadège Baumlin and Mélanie Tunis for performing *in vivo* experiments and biomarker analysis, Dr. G. Santiso-Quinones from Crystallise AG for crystallization experiments and preparation of files for the CSD, and Dr. Gianvito Vilé for the synthesis of some key intermediates by continuous flow chemistry.

■ ABBREVIATIONS USED

AcOH, acetic acid; BPR, back pressure regulator; CHO, Chinese hamster ovary; Cl_{int}, intrinsic clearance; clog $D_{7.4}$, calculated log *D* at pH 7.4; C_{max}, maximal (peak) plasma concentration; Compd, compound; DEA, diethylamine; DIPEA, diisopropylethylamine; DLM, dog liver microsomes; EtOAc, ethyl acetate; EtOH, ethanol; HATU, 2-(7-aza-1*H*-benzotriazole-1-yl)-1,1,3,3-tetramethyluronium hexafluorophosphate; HEPES, 4-(2-hydroxyethyl)-1-piperazineethanesulfonic acid; hERG, human ether-à-go-go related gene (also called hKV11.1); HLM, human liver microsomes; HTRF, homogeneous time resolved technology; hPPB, human plasma protein binding; HV, high vacuum; KO^{t}Bu, potassium *tert*-butoxide; log $D_{7.4}$, measured log *D* at pH 7.4; MeCN, acetonitrile; MeOH, methanol; $NaBH(OAc)_3$, sodium triacetoxyborohydride; NaOAc, sodium acetate; NaOEt, sodium ethanolate; nM, nanomolar; PDA, photo diode array; Pd(dppf)Cl_2·DCM, (1,1′-bis(diphenylphosphino)ferrocene) dichloropalladium (II) dichloromethane; p.o., per os; prep., preparative; QC, quality control; *rac*, racemic; RLM, rat liver microsomes; TBTU, 2-(1*H*-benzotriazole-1-yl)-1,2,3,3-tetramethyluronium tetrafluoroborate; $T_{1/2}$, terminal half-life; TEA, triethylamine; T_{max}, time of maximal plasma concentration; T_3P, propylphosphonic anhydride; UAS, Upstream Activation Sequence

■ REFERENCES

(1) Burns, J. M.; Summers, B. C.; Wang, Y.; Melikian, A.; Berahovich, R.; Miao, Z.; Penfold, M. E. T.; Sunshine, M. J.; Littman, D. R.; Kuo, C. J.; Wei, K.; McMaster, B. E.; Wright, K.; Howard, M. C.; Schall, T. J. A Novel Chemokine Receptor for SDF-1 and I-TAC Involved in Cell Survival, Cell Adhesion, and Tumor Development. *J. Exp. Med.* **2006**, *203*, 2201−2213.

(2) Banisadr, G.; Podojil, J. R.; Miller, S. D.; Miller, R. J. Pattern of CXCR7 Gene Expression in Mouse Brain Under Normal and Inflammatory Conditions. *J. Neuroimmune Pharmacol.* **2016**, *11*, 26−35.

(3) Balabanian, K.; Lagane, B.; Infantino, S.; Chow, K. Y. C.; Harriague, J.; Moepps, B.; Arenzana-Seisdedos, F.; Thelen, M.; Bachelerie, F. The Chemokine SDF-1/CXCL12 Binds to and Signals Through the Orphan Receptor RDC1 in T lymphocytes. *J. Biol. Chem.* **2005**, *280*, 35760−35766.

(4) Naumann, U.; Cameroni, E.; Pruenster, M.; Mahabaleshwar, H.; Raz, E.; Zerwes, H. G.; Rot, A.; Thelen, M. CXCR7 Functions as a Scavenger for CXCL12 and CXCL11. *PLoS One* **2010**, *5*, No. e9175.

(5) Sánchez-Alcañiz, J. A.; Haege, S.; Mueller, W.; Pla, R.; Mackay, F.; Schulz, S.; López-Bendito, G.; Stumm, R.; Marín, O. CXCR7 Controls Neuronal Migration by Regulating Chemokine Responsiveness. *Neuron* **2011**, *69*, 77−90.

(6) Zohar, Y.; Wildbaum, G.; Novak, R.; Salzman, A. L.; Thelen, M.; Alon, R.; Barsheshet, Y.; Karp, C. L.; Karin, N. CXCL11-Dependent Induction of FOXP3-Negative Regulatory T Cells Suppresses Autoimmune Encephalomyelitis. *J. Clin. Invest.* **2014**, *124*, 2009−2022.

(7) Tokunaga, R.; Zhang, W.; Naseem, M.; Puccini, A.; Berger, M. D.; Soni, S.; McSkane, M.; Baba, H.; Lenz, H. J. CXCL9, CXCL10, CXCL11/CXCR3 Axis for Immune Activation - a Target for Novel Cancer Therapy. *Cancer Treat. Rev.* **2018**, *63*, 40−47.

(8) Torraca, V.; Cui, C.; Boland, R.; Bebelman, J. P.; van der Sar, A. M.; Smit, M. J.; Siderius, M.; Spaink, H. P.; Meijer, A. H. The CXCR3-CXCL11 Signaling Axis Mediates Macrophage Recruitment and Dissemination of Mycobacterial Infection. *Dis. Model Mech.* **2015**, *8*, 253−269.

(9) Quinn, K. E.; Mackie, D. I.; Caron, K. M. Emerging Roles of Atypical Chemokine Receptor 3 (ACKR3) in Normal Development and Physiology. *Cytokine+* **2018**, *109*, 17−23.

(10) Wang, Y.; Huang, J.; Li, Y.; Yang, G. Y. Roles of Chemokine CXCL12 and its Receptors in Ischemic Stroke. *Curr. Drug Targets* **2012**, *13*, 166−172.

(11) Puchert, M.; Pelkner, F.; Stein, G.; Angelov, D. N.; Boltze, J.; Wagner, D. C.; Odoardi, F.; Flügel, A.; Streit, W. J.; Engele, J. Astrocytic Expression of the CXCL12 Receptor, CXCR7/ACKR3 is a Hallmark of the Diseased, but not Developing CNS. *Mol. Cell. Neurosci.* **2017**, *85*, 105−118.

(12) Xu, T.; Yu, X.; Deng, J.; Ou, S.; Liu, X.; Wang, T.; Liu, Y.; Yang, J.; Tan, C.; Yuan, J.; Chen, Y. CXCR7 Regulates Epileptic Seizures by Controlling the Synaptic Activity of Hippocampal Granule Cells. *Cell Death Dis.* **2019**, *10*, 825.

(13) Trojan, E.; Ślusarczyk, J.; Chamera, K.; Kotarska, K.; Glombik, K.; Kubera, M.; Basta-Kaim, A. The Modulatory Properties of Chronic Antidepressant Drugs Treatment on the Brain Chemokine - Chemokine Receptor Network: A Molecular Study in an Animal Model of Depression. *Front. Pharmacol.* **2017**, *8*, 779.

(14) McCandless, E. E.; Piccio, L.; Woerner, B. M.; Schmidt, R. E.; Rubin, J. B.; Cross, A. H.; Klein, R. S. Pathological Expression of CXCL12 at the Blood-Brain Barrier Correlates with Severity of Multiple Sclerosis. *Am. J. Pathol.* **2008**, *172*, 799−808.

(15) Moll, N. M.; Cossoy, M. B.; Fisher, E.; Staugaitis, S. M.; Tucky, B. H.; Rietsch, A. M.; Chang, A.; Fox, R. J.; Trapp, B. D.; Ransohoff, R. M. Imaging Correlates of Leukocyte Accumulation and CXCR4/CXCL12 in Multiple Sclerosis. *Arch. Neurol.* **2009**, *66*, 44−53.

(16) Cruz-Orengo, L.; Holman, D. W.; Dorsey, D.; Zhou, L.; Zhang, P.; Wright, M.; McCandless, E. E.; Patel, J. R.; Luker, G. D.; Littman, D. R.; Russell, J. H.; Klein, R. S. CXCR7 Influences Leukocyte Entry into the CNS Parenchyma by Controlling Abluminal CXCL12 Abundance During Autoimmunity. *J. Exp. Med.* **2011**, *208*, 327−339.

(17) Watanabe, K.; Penfold, M. E. T.; Matsuda, A.; Ohyanagi, N.; Kaneko, K.; Miyabe, Y.; Matsumoto, K.; Schall, T. J.; Miyasaka, N.; Nanki, T. Pathogenic Role of CXCR7 in Rheumatoid Arthritis. *Arthritis Rheum.* **2010**, *62*, 3211−3220.

(18) Konrad, F. M.; Meichssner, N.; Bury, A.; Ngamsri, K. C.; Reutershan, J. Inhibition of SDF-1 Receptors CXCR4 and CXCR7 Attenuates Acute Pulmonary Inflammation via the Adenosine A2B-Receptor on Blood Cells. *Cell Death Dis.* **2017**, *8*, No. e2832.

https://dx.doi.org/10.1021/acs.jmedchem.0c01588
J. Med. Chem. XXXX, XXX, XXX−XXX

(19) Ngamsri, K.-C.; Müller, A.; Bösmüller, H.; Gamper-Tsigaras, J.; Reutershan, J.; Konrad, F. M. The Pivotal Role of CXCR7 in Stabilization of the Pulmonary Epithelial Barrier in Acute Pulmonary Inflammation. *J. Immunol.* **2017**, *198*, 2403−2413.
(20) Chang, H.-C.; Huang, P.-H.; Syu, F.-S.; Hsieh, C.-H.; Chang, S. L.-Y.; Lu, J.; Chen, H.-C. Critical Involvement of Atypical Chemokine Receptor CXCR7 in Allergic Airway Inflammation. *Immunology* **2018**, *154*, 274−284.
(21) Wang, C.; Chen, W.; Shen, J. CXCR7 Targeting and Its Major Disease Relevance. *Front. Pharmacol.* **2018**, *9*, 641.
(22) Walters, M. J.; Ebsworth, K.; Berahovich, R. D.; Penfold, M. E. T.; Liu, S.-C.; Al Omran, R.; Kioi, M.; Chernikova, S. B.; Tseng, D.; Mulkearns-Hubert, E. E.; Sinyuk, M.; Ransohoff, R. M.; Lathia, J. D.; Karamchandani, J.; Kohrt, H. E. K.; Zhang, P.; Powers, J. P.; Jaen, J. C.; Schall, T. J.; Merchant, M.; Recht, L.; Brown, J. M. Inhibition of CXCR7 Extends Survival Following Irradiation of Brain Tumours in Mice and Rats. *Br. J. Cancer* **2014**, *110*, 1179−1188.
(23) Guillemot, E.; Karimdjee-Soilihi, B.; Pradelli, E.; Benchetrit, M.; Goguet-Surmenian, E.; Millet, M. A.; Larbret, F.; Michiels, J. F.; Birnbaum, D.; Alemanno, P.; Schmid-Antomarchi, H.; Schmid-Alliana, A. CXCR7 Receptors Facilitate the Progression of Colon Carcinoma within Lung not within Liver. *Br. J. Cancer* **2012**, *107*, 1944−1949.
(24) Luker, K. E.; Lewin, S. A.; Mihalko, L. A.; Schmidt, B. T.; Winkler, J. S.; Coggins, N. L.; Thomas, D. G.; Luker, G. D. Scavenging of CXCL12 by CXCR7 Promotes Tumor Growth and Metastasis of CXCR4-Positive Breast Cancer Cells. *Oncogene* **2012**, *31*, 4750−4758.
(25) Goguet-Surmenian, E.; Richard-Fiardo, P.; Guillemot, E.; Benchetrit, M.; Gomez-Brouchet, A.; Buzzo, P.; Karimdjee-Soilihi, B.; Alemanno, P.; Michiels, J. F.; Schmid-Alliana, A.; Schmid-Antomarchi, H. CXCR7-Mediated Progression of Osteosarcoma in the Lungs. *Br. J. Cancer* **2013**, *109*, 1579−1585.
(26) Wani, N. A.; Nasser, M. W.; Ahirwar, D. K.; Zhao, H.; Miao, Z.; Shilo, K.; Ganju, R. K. C-X-C Motif Chemokine 12/C-X-C Chemokine Receptor Type 7 Signaling Regulates Breast Cancer Growth and Metastasis by Modulating the Tumor Microenvironment. *Breast Cancer Res.* **2014**, *16*, R54.
(27) Sierro, F.; Biben, C.; Martinez-Munoz, L.; Mellado, M.; Ransohoff, R. M.; Li, M.; Woehl, B.; Leung, H.; Groom, J.; Batten, M.; Harvey, R. P.; Martinez-A, C.; Mackay, C. R.; Mackay, F. Disrupted Cardiac Development But Normal Hematopoiesis in Mice Deficient in the Second CXCL12/SDF-1 Receptor, CXCR7. *Proc. Natl. Acad. Sci. U. S. A.* **2007**, *104*, 14759−14764.
(28) Menhaji-Klotz, E.; Hesp, K. D.; Londregan, A. T.; Kalgutkar, A. S.; Piotrowski, D. W.; Boehm, M.; Song, K.; Ryder, T.; Beaumont, K.; Jones, R. M.; Atkinson, K.; Brown, J. A.; Litchfield, J.; Xiao, J.; Canterbury, D. P.; Burford, K.; Thuma, B. A.; Limberakis, C.; Jiao, W.; Bagley, S. W.; Agarwal, S.; Crowell, D.; Pazdziorko, S.; Ward, J.; Price, D. A.; Clerin, V. Discovery of a Novel Small-Molecule Modulator of C-X-C Chemokine Receptor Type 7 as a Treatment for Cardiac Fibrosis. *J. Med. Chem.* **2018**, *61*, 3685−3696.
(29) Dong, B. C.; Li, M. X.; Wang, X. Y.; Cheng, X.; Wang, Y.; Xiao, T.; Jolkkonen, J.; Zhao, C. S.; Zhao, S. S. Effects of CXCR7-Neutralizing Antibody on Neurogenesis in the Hippocampal Dentate Gyrus and Cognitive Function in the Chronic Phase of Cerebral Ischemia. *Neural Regener. Res.* **2020**, *15*, 1079−1085.
(30) Bao, J.; Zhu, J.; Luo, S.; Cheng, Y.; Zhou, S. CXCR7 Suppression Modulates Microglial Chemotaxis to Ameliorate Experimentally-Induced Autoimmune Encephalomyelitis. *Biochem. Biophys. Res. Commun.* **2016**, *469*, 1−7.
(31) Peng, H.; Zhang, H.; Zhu, H. Blocking CXCR7-Mediated Adipose Tissue Macrophages Chemotaxis Attenuates Insulin Resistance and Inflammation in Obesity. *Biochem. Biophys. Res. Commun.* **2016**, *479*, 649−655.
(32) Salazar, N.; Carlson, J. C.; Huang, K.; Zheng, Y.; Oderup, C.; Gross, J.; Jang, A. D.; Burke, T. M.; Lewén, S.; Scholz, A.; Huang, S.; Nease, L.; Kosek, J.; Mittelbronn, M.; Butcher, E. C.; Tu, H.; Zabel, B. A. A Chimeric Antibody Against ACKR3/CXCR7 in Combination with TMZ Activates Immune Responses and Extends Survival in Mouse GBM Models. *Mol. Ther.* **2018**, *26*, 1354−1365.
(33) Maussang, D.; Mujić-Delić, A.; Descamps, F. J.; Stortelers, C.; Vanlandschoot, P.; Walsum, M. S.-v.; Vischer, H. F.; van Roy, M.; Vosjan, M.; Gonzalez-Pajuelo, M.; van Dongen, G. A.; Merchiers, P.; van Rompaey, P.; Smit, M. J. Llama-Derived Single Variable Domains (Nanobodies) Directed Against Chemokine Receptor CXCR7 Reduce Head and Neck Cancer Cell Growth in vivo. *J. Biol. Chem.* **2013**, *288*, 29562−29572.
(34) Zabel, B. A.; Wang, Y.; Lewén, S.; Berahovich, R. D.; Penfold, M. E. T.; Zhang, P.; Powers, J.; Summers, B. C.; Miao, Z.; Zhao, B.; Jalili, A.; Janowska-Wieczorek, A.; Jaen, J. C.; Schall, T. J. Elucidation of CXCR7-Mediated Signaling Events and Inhibition of CXCR4-Mediated Tumor Cell Transendothelial Migration by CXCR7 Ligands. *J. Immunol.* **2009**, *183*, 3204−3211.
(35) Luker, K. E.; Gupta, M.; Luker, G. D. Imaging Chemokine Receptor Dimerization with Firefly Luciferase Complementation. *FASEB J.* **2008**, *23*, 823−834.
(36) Gustavsson, M.; Wang, L.; van Gils, N.; Stephens, B. S.; Zhang, P.; Schall, T. J.; Yang, S.; Abagyan, R.; Chance, M. R.; Kufareva, I.; Handel, T. M. Structural Basis of Ligand Interaction with Atypical Chemokine Receptor 3. *Nat. Commun.* **2017**, *8*, 14135.
(37) Menhaji-Klotz, E.; Ward, J.; Brown, J. A.; Loria, P. M.; Tan, C.; Hesp, K. D.; Riccardi, K. A.; Litchfield, J.; Boehm, M. Discovery of Diphenylacetamides as CXCR7 Inhibitors with Novel β-Arrestin Antagonist Activity. *ACS Med. Chem. Lett.* **2020**, *11*, 1330−1334.
(38) Fretz, H. G.; Guerry, P.; Kimmerlin, T.; Lehembre, F.; Pfeifer, T.; Valdenaire, A. 1 -[m-Carboxamido(hetero)aryl-methyl]-piperidine-4-carboxamide Derivatives as CXCR7 Modulators and their Preparation. US20130345199A1, 2013.
(39) Waring, M. J. Lipophilicity in Drug Discovery. *Expert Opin. Drug Discov.* **2010**, *5*, 235−248.
(40) Meanwell, N. A. Fluorine and Fluorinated Motifs in the Design and Application of Bioisosteres for Drug Design. *J. Med. Chem.* **2018**, *61*, 5822−5880.
(41) Schinnerl, M.; Murray, J. K.; Langenhan, J. M.; Gellman, S. H. Asymmetric Synthesis of a New Helix-Forming β-Amino Acid: trans-4-Aminopiperidine-3-carboxylic Acid. *Eur. J. Org. Chem.* **2003**, 721−726.
(42) Sheldrick, G. M. SHELXT - Integrated Space-Group and Crystal-Structure Determination. *Acta Crystallogr. A Found Adv.* **2015**, *71*, 3−8.
(43) Sheldrick, G. M. Crystal Structure Refinement with SHELXL. *Acta Crystallogr. C Struct. Chem.* **2015**, *71*, 3−8.
(44) Spek, A. L. PLATONSQUEEZE: A Tool for the Calculation of the Disordered Solvent Contribution to the Calculated Structure Factors. *Acta Crystallogr., Sect. C* **2015**, *71*, 9−18.

https://dx.doi.org/10.1021/acs.jmedchem.0c01588
J. Med. Chem. XXXX, XXX, XXX−XXX